CERN/PS 87-9 (BT)
(1987)

A 1.5 GHz WIDE-BAND BEAM-POSITION-AND-INTENSITY MONITOR FOR THE ELECTRON-POSITRON ACCUMULATOR (EPA)

G.C. Schneider

ABSTRACT

A resistive beam monitor was developed for the observation of transverse and longitudinal microwave instabilities and for bunch length (σ = 0.7 ns) measurements. The relevant equations are derived, analysed, and optimized. The electrical and mechanical layouts are given as well as the characteristics of the monitor. The signals for horizontal and vertical beam-position and for intensity have a rise-time of $\leq$ 230 ps at the end of 100 m transmission cables. Cable losses are compensated by computer-optimized filters. The peak intensity signal is 2.7 V for the nominal beam intensity of 2.5 x 10^{10} e^+/e^- particles per bunch. At 40 mm off centre, the position signals equal the intensity signal. A laboratory set-up allows the transverse displacement of a rod or wire in a 3 m long, cylindrical chamber. Time filtering prevents perturbation through imperfect matching at the end of the tube for off-centre wire positions. Results obtained with the laboratory set-up and with real beams in the accumulator ring are presented.

Contents

		Page
1.	INTRODUCTION AND REQUIREMENTS	1
2.	THEORY	1
	2.1 Four-point pick-up with uniformly conducting ring	3
	2.2 Pick-up with a ring of lumped resistors	9
	2.3 Signal propagation on the lossy transverse gap line	11
	2.3.1 Low-frequency limit of the difference signal	11
	2.3.2 Low-frequency limit of the sum signal	13
	2.3.3 Upper-frequency limit	13
	2.4 The frequency-dependent transfer functions of the monitor	17
	2.5 Signal transmission and optimization	21
3.	MECHANICAL DESIGN	27
4.	TEST BENCH	29
	4.1 Mechanical test device	29
	4.2 Laboratory results	31
5.	RESULTS WITH BEAM	33
6.	CLOSING REMARKS	35
7.	CHARACTERISTICS	36
APPENDIX 1:	Derivation of sum of Q versus beam positions r and χ	37
APPENDIX 2:	Integration of the charge-distribution integral	39
APPENDIX 3:	Lower cut-off frequency of the beam-position signal	41
APPENDIX 4:	Filter transfer function	45
APPENDIX 5:	A) FORTRAN subroutine of 'MINUIT' program for pick-up sum signal optimization B) Output of 'MINUIT' optimization program (sum signal)	47
APPENDIX 6:	A) Complex transfer function of 'LAPLACE' program for sum signal transmission with optimum filter parameters (3 ns rectangular input) B) Complex transfer function for optimum filter parameters (3 ns triangular input)	48

APPENDIX 7: A) FORTRAN subroutine of 'MINUIT' for difference signal optimization 50
B) 'MINUIT' output difference signal optimization

APPENDIX 8: A) Complex transfer function 'LAPLACE' for difference signal transmission with optimum filter parameters (3 ns rectangular input) 51
B) Complex transfer function for optimum filter parameters (3 ns triangular input)

REFERENCES 53

1. INTRODUCTION AND REQUIREMENTS

This monitor was developed for the electron-positron accumulator (EPA) ring to observe the fast longitudinal and transverse behaviour of the bunches during acceleration and stacking. Of special interest are the microwave instabilities. The accelerated bunches have a bunch length of about 3 ns. It was decided that a 300 ps monitor rise-time, corresponding to ~ 1 GHz, would be sufficient for analysing the longitudinal bunch structure. The lower frequency limit was fixed at 10 MHz, as other pick-ups cover the lower frequency range.

The nominal beam intensity per bunch for e^+ (e^-) is 2.5 (1.25) x 10^{10} particles per bunch (ppb), which corresponds to a peak current of 2.2 (1.1) A [1]. A dynamic of 10^3 was specified to cover the intensity range of $10^8 < I < 10^{11}$ ppb.

The beam coupling impedances $|Z/n|$ should not exceed 0.2 Ω.

Because of the desired flat frequency response up to 1 GHz, the monitor was chosen of the resistive type, where a short length of the vacuum chamber is replaced by a uniformly resistive ring. The voltage distribution across this ring, induced by the image current of the beam, contains all information about the beam position and intensity.

2. THEORY

A charged-particle bunch moving with a highly relativistic speed in a well-conducting vacuum chamber is accompanied by a pure transverse electric field. The induced charge distribution of the image current on a circular chamber wall versus beam position is well known [2-6]

$$q(r,\varphi,X) = \frac{1 - r^2}{1 + r^2 - 2r\cos(\varphi - X)} . \qquad (1)$$

The parameters are shown in Fig. 1, where the chamber is represented as the unit circle in the x-y plane:

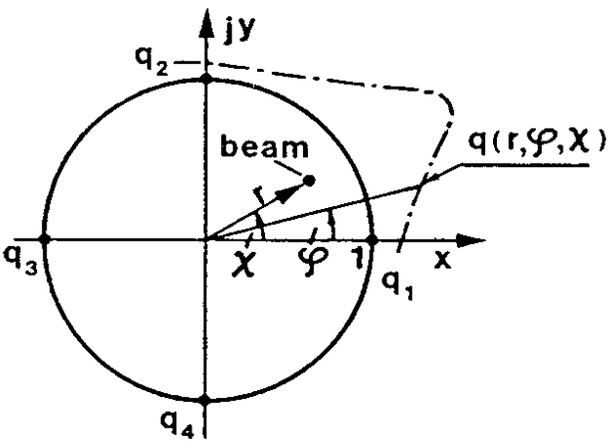

Fig. 1 Off-centre beam in circular chamber

The beam position is given by the complex vector

$$\underline{r} = r\, e^{j\chi} \,, \tag{2}$$

with

$$y = r \sin \chi \tag{3a}$$

$$x = r \cos \chi \tag{3b}$$

and

$$x^2 + y^2 = r^2 \,. \tag{3c}$$

The charge density q appears over the azimuthal angle φ. Figure 2 shows the charge density versus φ [from Eq. (1)] for a centred beam

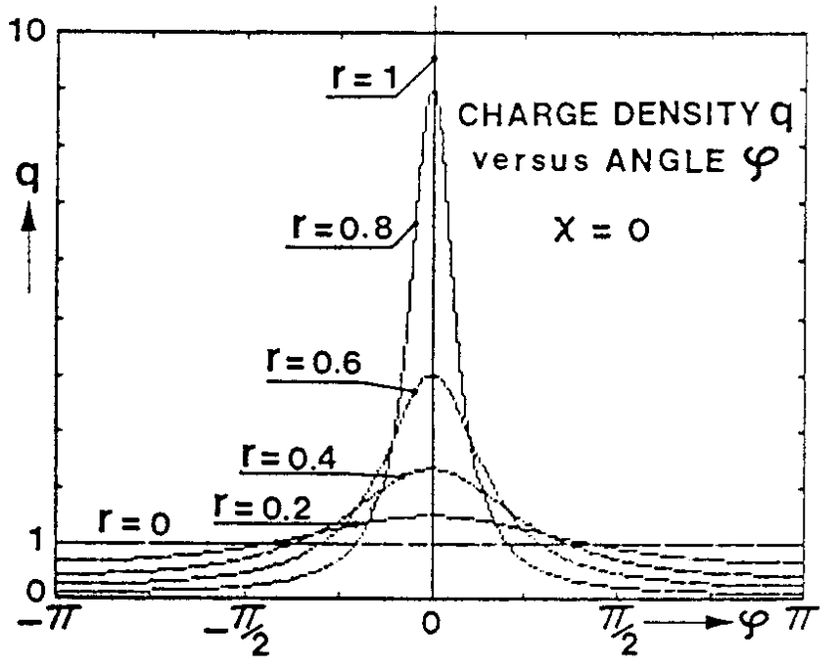

Fig. 2 Charge density versus angle φ

(r = 0) and five off-centre beam positions r = 0 to r = 1 on the real axis (X = 0).

The integral

$$\int_{-\pi}^{\pi} q(r,\varphi)\, d\varphi = 2\pi \qquad (4)$$

is a constant for all beam positions r. This can easily be seen for r = 0, where the charge distribution q is uniform and equal to 1. But Eq. (4) is also valid for r = 1, where q(0) is infinite, if the total charge of the beam is the same in both cases.

2.1 Four-point pick-up with uniformly conducting ring

Knowledge of the chamber image current at the four axis points is sufficient to determine the beam position and intensity. These four currents are measured by means of a resistive ring inserted in the vacuum chamber (see Fig. 11).

Consider the four charge densities q_1, q_2, q_3, and q_4 on the axis for $\varphi = 0$, $\pi/2$, π, and $3\pi/2$ created by a beam in position r (Fig. 1). From Eq. (1), for $\varphi = 0$, π, $\pi/2$, and $3\pi/2$, these charge densities are respectively

$$q_1 = \frac{1 - r^2}{1 + r^2 - 2r \cos(-X)}, \qquad (5)$$

$$q_3 = \frac{1 - r^2}{1 + r^2 - 2r \cos(\pi - X)}, \qquad (6)$$

$$q_2 = \frac{1 - r^2}{1 + r^2 - 2r \cos[(\pi/2) - X]}, \qquad (7)$$

$$q_4 = \frac{1 - r^2}{1 + r^2 - 2r \cos[(3/2)\pi - X]}, \qquad (8)$$

Equations (5) to (8) can be written in a shorter form:

$$q_\nu = \frac{1 - r^2}{1 + r^2 - 2r \cos\left[\frac{\pi}{2}(\nu - 1) - X\right]}. \qquad (9)$$

with ν = 1, 2, 3, 4.

a) *The difference charge* [Eqs. (5) and (6)] is

$$\boxed{q_1 - q_3 = \Delta q_{13} = \frac{(1 - r^2)\, 4r \cos \chi}{(1 + r^2)^2 - 4r^2 \cos^2 \chi}} \tag{10a}$$

or, with Eqs. (3) in Cartesian coordinates,

$$\Delta q_{13}(x,y) = \frac{(1 - x^2 - y^2)\, 4x}{(1 + x^2 + y^2) - 4x^2} \,. \tag{10b}$$

Similarly, from Eqs. (7) and (8),

$$q_2 - q_4 = \Delta q_{24} = \frac{(1 - r^2)\, 4r \sin \chi}{(1 + r^2)^2 - 4r^2 \sin^2 \chi} \,, \tag{11}$$

or, with Eqs. (3a) and (3c),

$$\Delta q_{24}(x,y) = \frac{(1 - x^2 - y^2)\, 4y}{(1 + x^2 + y^2) - 4y^2} \,. \tag{12}$$

The sensitivities in the x and y directions are equal, as from Eqs. (10b) and (12),

$$\frac{\partial \Delta q_{13}}{\partial x} = \frac{\partial \Delta q_{24}}{\partial y} \,. \tag{13}$$

Figure 3 gives a three-dimensional perspective presentation of the function Eqs. (10a, b). It can be seen that the slope of the Δq_{13} surface in the x direction is maximum for y = 0 and minimum for y = $\pm$1.

```
 5 ! "DELTAQ"          HP 85
 12 P=-1
 14 T=.5
 20 SCALE -1,1,-5.5
 30 XAXIS 0,0
 40 YAXIS 0,0
 60 GOSUB 1500
 90 GOSUB 2000
 95 BEEP
100 END
161 !
1000 REM PERSPECTIVE
1060 X=R*COS(T+C)
1065 Y=Q*COS(P)-R*SIN(T+C)*SIN(P
     )
1070 RETURN
1071 !
1500 REM CIRCUMFERENCE
1510 FOR R=.2 TO 1 STEP .2
1520 FOR C=0 TO 2*PI STEP PI/20
1530 GOSUB 3000
1540 GOSUB 1000
1550 IF C=0 THEN MOVE X,Y
1560 PLOT X,2*Y
1570 NEXT C
1580 NEXT R
1600 RETURN
1601 !
2000 REM RADIUS
2010 FOR C=0 TO 2*PI STEP PI/8
2020 FOR R=0 TO 1 STEP .1
2025 GOSUB 3000
2030 GOSUB 1000
2035 IF R=0 THEN MOVE X,Y
2040 PLOT X,2*Y
2050 NEXT R
2060 NEXT C
2070 RETURN
2071 !
3000 REM FUNCTION
3010 Z=4*R*(1-R*R)*COS(C)
3020 N=(1+R*R)^2-4*R*R*COS(C)^2
3030 IF N=0 THEN GOTO 3050
3040 Q=Z/N
3050 RETURN
```

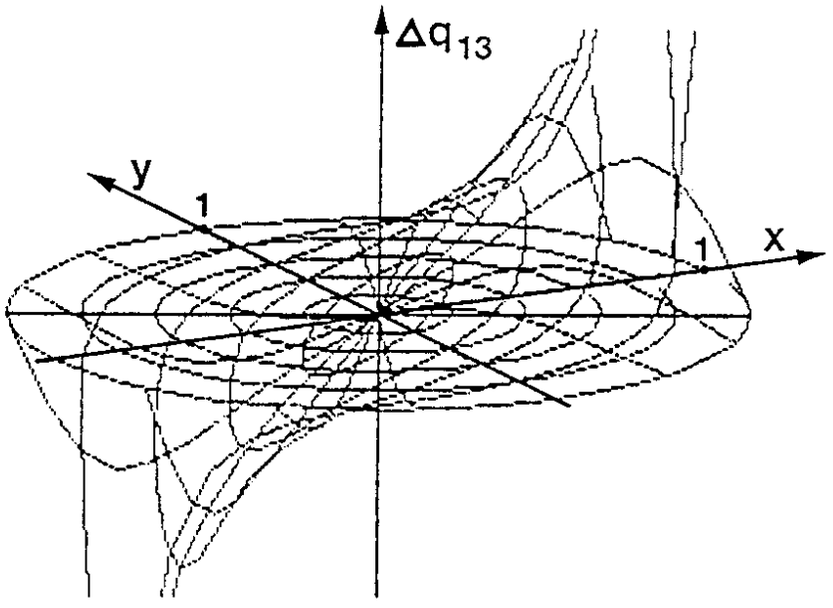

Fig. 3 Difference signal Δq_{13} versus beam position (r,X)

b) *The sum of the four point charges* Eqs. (5) to (8),

$$\Sigma q = q_1 + q_2 + q_3 + q_4 \ ,$$

is calculated in Appendix 1:

$$\Sigma q(r,X) = \frac{4(1 - r^8)}{(1 - r^4)^2 + 16r^4 \cos^2 X \sin^2 X} \ . \qquad (14)$$

Figure 4 gives the three-dimensional perspective representation of Σq (Σq is constant equal 4 for small r).

```
  5 ' "SIGMA0"
 12 P=-1.1
 14 T=.5
 20 SCALE -1,1,-2.5
 30 XAXIS 0,0
 40 YAXIS 0,0
 60 GOSUB 1500
 90 GOSUB 2000
 95 BEEP
100 END
101 '
1000 REM PERSPECTIVE
1060 X=R*COS(T+C)
1065 Y=Q*COS(P)-R*SIN(T+C)*SIN(P
     )
1070 RETURN
1071 '
1500 REM CIRCUMFERENCE
1510 FOR R=.2 TO 1 STEP .2
1520 FOR C=0 TO 2*PI STEP PI/30
1530 GOSUB 3000
1540 GOSUB 1000
1550 IF C=0 THEN MOVE X,Y
1560 PLOT X,2*Y
1570 NEXT C
1580 NEXT R
1600 RETURN
1601 '
2000 REM RADIUS
2010 FOR C=0 TO 2*PI STEP PI/8
2020 FOR R=0 TO 1 STEP .05
2025 GOSUB 3000
2030 GOSUB 1000
2035 IF R=0 THEN MOVE X,Y
2040 PLOT X,2*Y
2050 NEXT R
2060 NEXT C
2070 RETURN
2071 '
3000 REM FUNCTION
3010 Z=4*(1-R^8)
3020 N=(1-R^4)^2+16*R^4*COS(C)^2
     *SIN(C)^2
3030 IF N=0 THEN GOTO 3050
3040 Q=Z/N
3050 RETURN
```

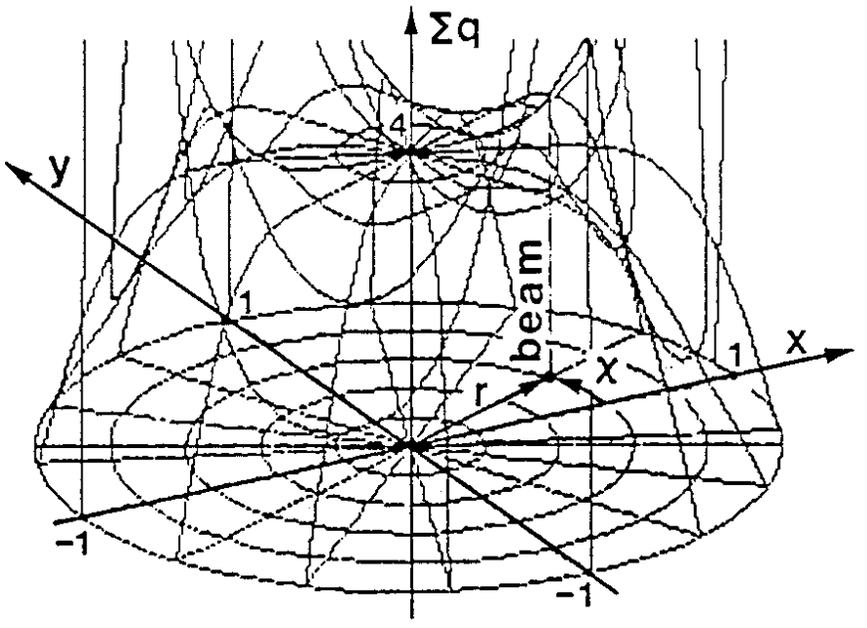

Fig. 4 Sum signal Σq versus beam position (r,x)

Figure 5 shows the projection of Σq in the x - Σq plane (tilt and rotation = 0) with r as the parameter. The error of Σq is about ±5% for r ≤ 0.4.

```
  5 ' "SIGMA0"
 12 P=0
 14 T=0
 20 SCALE -1,1,0.10
 30 XAXIS 0,.1
 40 YAXIS 0,0
 60 GOSUB 1500
 90 GOSUB 2000
 95 BEEP
100 END
101 '
```

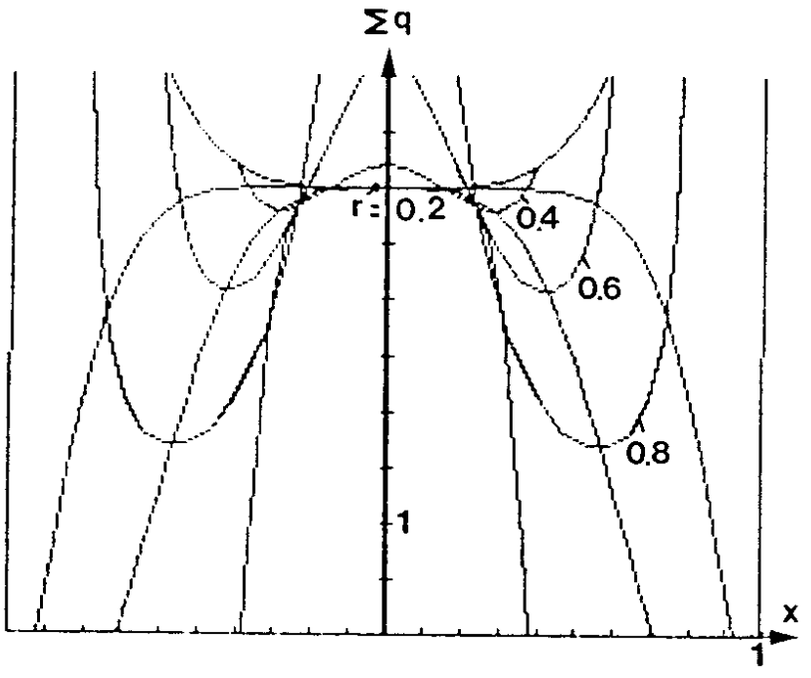

Fig. 5 Sum signal Σq(r,x) projected in the x-Σq plane

c) *The normalized beam-position signal* is, from Eqs. (10a) and (14):

$$\frac{\Delta q}{\Sigma q} = \frac{r \cos \chi \left[(1 - r^4)^2 + 16\, r^4 \cos^2 \chi \sin^2 \chi\right]}{\left[(1 + r^2)^2 - 4r^2 \cos^2 \chi\right](1 + r^2 + r^4 + r^6)} \qquad (15)$$

or in Cartesian coordinates with Eq. (3),

$$\frac{\Delta q}{\Sigma q}(x,y) = \frac{x\{[1 - (x^2 + y^2)]^2 + 16x^2y^2\}}{[(1 + x^2 + y^2)^2 - 4x^2](1 + x^2 + y^2)[1 + (x^2 + y^2)^2]} . \qquad (16)$$

This function has a constant slope r cos χ in the x direction for small r (Fig. 6).

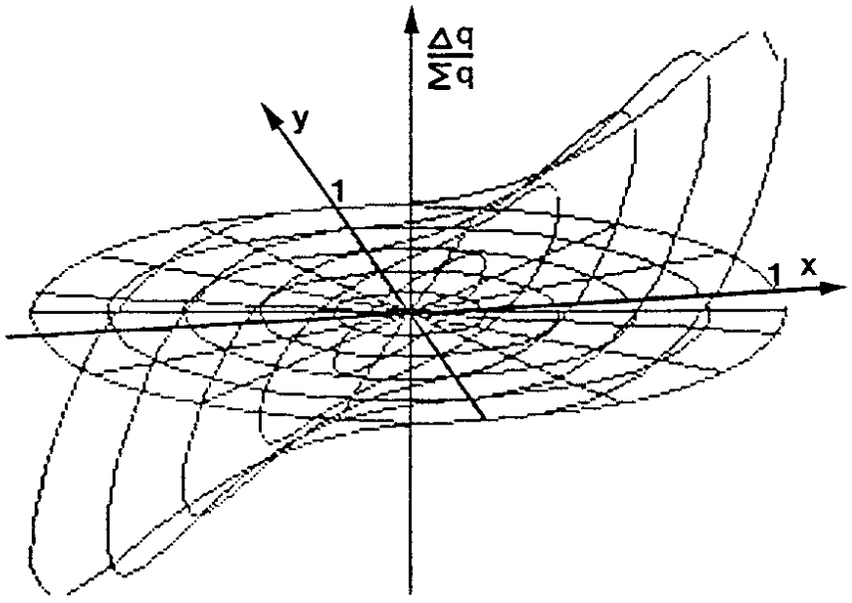

Fig. 6 Position signal Δq/Σq versus beam position (r,χ) or (x,y)

d) *The linearity error* ε in the x direction

$$\varepsilon = \frac{(\Delta q/\Sigma q) - x}{x} = \frac{\Delta q}{\Sigma q \cdot x} - 1 \qquad (17)$$

and with Eqs. (15) and (3b)

$$\varepsilon = \frac{(1 - r^4)^2 + 16r^4 \cos^2 \chi \sin^2 \chi}{[(1 + r^2)^2 - 4r^2 \cos^2 \chi](1 + r^2 + r^4 + r^6)} - 1. \qquad (18)$$

Equation (18) is represented in Fig. 7 as the projection in the x-ε plane for various r parameters. From this figure, there is a $\simeq$ 12% error for $|x| \leq 0.4$ and $|y| \leq 0.2$.

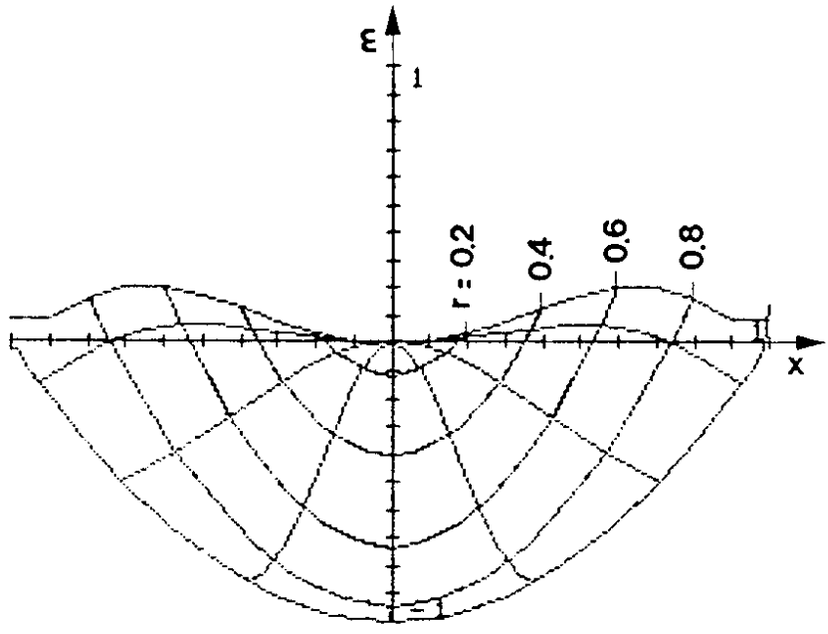

Fig. 7 Error function $\varepsilon(r,\chi)$ projected in the x-ε plane

The linearity error referred to the full scale $x_{max} = 1$

$$\varepsilon_f = \frac{[(\Delta q/\Sigma q) - x]}{x_{max}} \qquad (19)$$

is plotted in Fig. 8.

This error, normally given for instruments used for measurements is ±5% for a range $|r| \leq 0.4$.

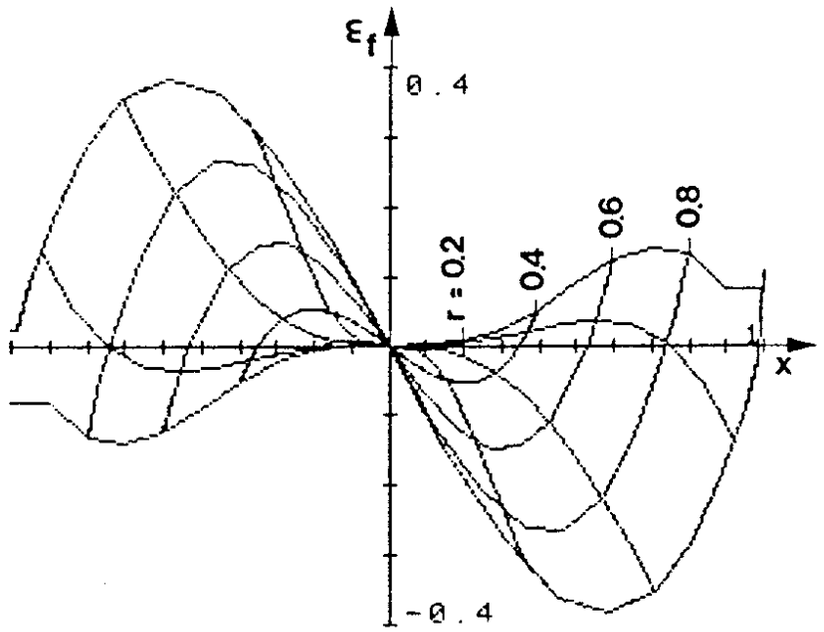

Fig. 8 Full-scale error function ε_f projected in x-ε_f plane

2.2 Pick-up with a ring of lumped resistors

A pick-up is considered where the uniformly conducting ring is replaced by N resistors (Fig. 9). The image charges Q_ν (ν = 1, 2,

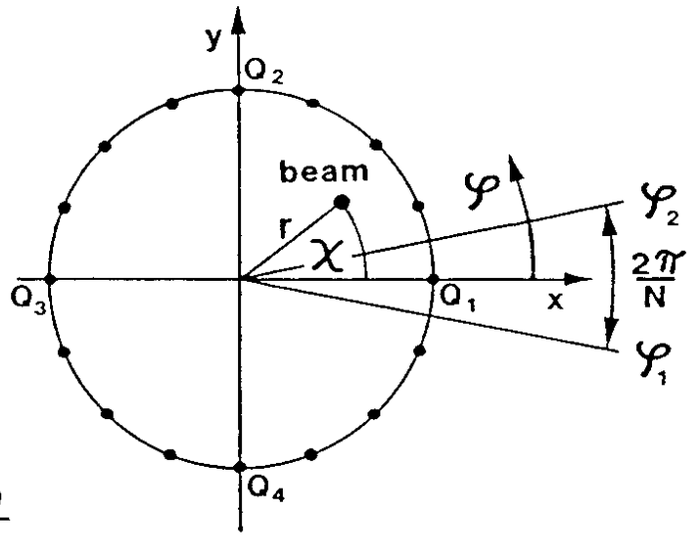

Fig. 9

3, 4) flowing through the four axis resistors can be obtained by integrating Eq. (1):

$$Q_v = \int_{\varphi_1}^{\varphi_2} q \cdot d\varphi = \int_{\varphi_1}^{\varphi_2} \frac{(1 - r^2)\, d\varphi}{1 + r^2 - 2r \cos(\varphi - \chi)} , \tag{20}$$

where the integration limits are for

$$\left.\begin{aligned} Q_1: &\quad \varphi_1 = -\frac{\pi}{N} ; &\quad \varphi_2 = \frac{\pi}{N} , \\ Q_2: &\quad \varphi_1 = \frac{\pi}{2} - \frac{\pi}{N} ; &\quad \varphi_2 = \frac{\pi}{2} + \frac{\pi}{N} , \\ Q_3: &\quad \varphi_1 = \pi - \frac{\pi}{N} ; &\quad \varphi_2 = \pi + \frac{\pi}{N} , \\ Q_4: &\quad \varphi_1 = \frac{3}{2}\pi - \frac{\pi}{N} ; &\quad \varphi_2 = \frac{3}{2}\pi + \frac{\pi}{N} . \end{aligned}\right\} \tag{21}$$

The integral of Eq. (20) can be solved analytically (see Appendix 2):

$$Q_v = 2\left\{\operatorname{arctg}\left[\frac{1 + r}{1 - r} \operatorname{tg}\left\{\frac{\varphi_2 - \chi}{2}\right\}\right] - \operatorname{arctg}\left[\frac{1 + r}{1 - r} \operatorname{tg}\left\{\frac{\varphi_1 - \chi}{2}\right\}\right]\right\} , \tag{22}$$

with φ_1 and φ_2 given in Eq. (21).

The difference between the opposite charges Q_1 and Q_3 can be calculated from Eqs. (22) and (21):

$$\Delta Q = Q_1 - Q_3 . \tag{23}$$

For the example N = 32 resistors, this function ΔQ is plotted in Fig. 10. Comparing ΔQ of Fig. 10 with Δq of Fig. 3 (uniformly

```
  5 ! "DELQ"
 12 P=-.3
 14 T=.25
 20 SCALE -1.1,-1.1
 30 ! XAXIS 0,0
 40 ! YAXIS 0,0
 60 GOSUB 1500
 90 GOSUB 2000
 95 BEEP
100 END
101 !
1000 REM PERSPECTIVE
1060 X=R*COS(T+C)
1065 Y=Q*COS(P)-R*SIN(T+C)*SIN(P
     )
1070 RETURN
1071 !
1500 REM CIRCUMFERENCE
1510 FOR R=.2 TO 1 STEP .199
1520 FOR C=-PI TO PI STEP PI/20
1530 GOSUB 3000
1540 GOSUB 1000
1550 IF C=-PI THEN MOVE X,Y
1560 PLOT X,2*Y
1570 NEXT C
1580 NEXT R
1600 RETURN
1601 !
2000 REM RADIUS
2010 FOR C=-PI TO PI STEP PI/8
2020 FOR R=.01 TO .99 STEP .098
2025 GOSUB 3000
2030 GOSUB 1000
2035 IF P<.1 THEN MOVE X,Y
2040 PLOT X,2*Y
2050 NEXT R
2060 NEXT C
2070 RETURN
2071 !
3000 REM FUNCTION
3010 Z=ATN((1+R)*TAN(PI/64-C/2)/
     (1-R))
3012 Z=Z-ATN((1+R)*TAN(-(PI/64)-
     C/2)/(1-R))
3014 Z=Z-ATN((1+R)*TAN(33*PI/64-
     C/2)/(1-R))
3016 Z=Z+ATN((1+R)*TAN(31*PI/64-
     C/2)/(1-R))
3018 IF Z>.8*PI THEN Z=Z-PI
3019 IF Z<-(.8*PI) THEN Z=Z+PI
3020 M=1
3030 IF M=0 THEN GOTO 3050
3040 Q=Z/N
3050 RETURN
```

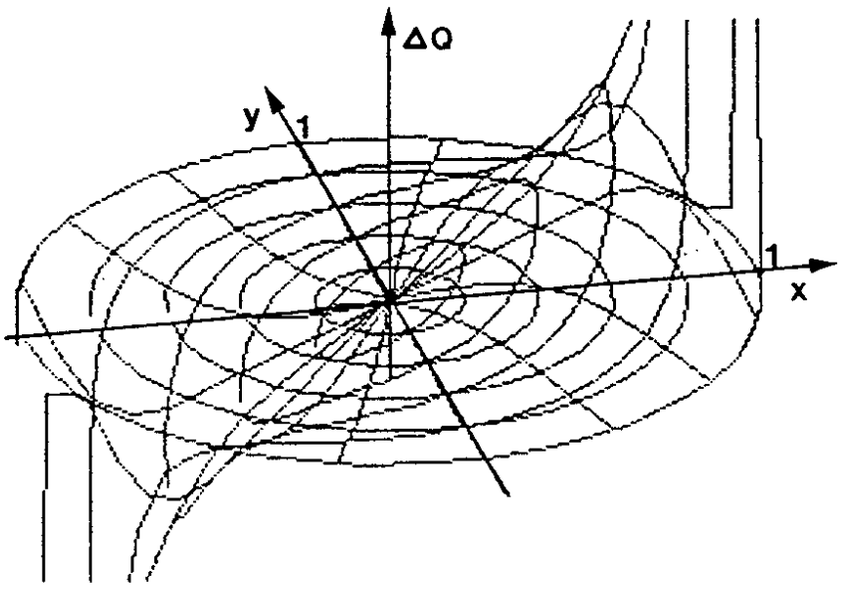

Fig. 10 Difference signal versus beam position (x,y)

conducting ring), a good similarity is noticed although the corresponding functions, Eqs. (9) and (22) resp. Eqs. (10a) and (23), are completely different.

The functions

$$\Sigma Q = Q_1 + Q_2 + Q_3 + Q_4 \ , \qquad (24)$$

$\Delta Q/\Sigma Q$, and ε can be computed correspondingly from Eqs. (22) and (21).

For a sufficiently high number N of resistors the values of the functions considered above approach, more and more, those of the uniformly conducting ring.

2.3 Signal propagation on the lossy transverse gap line

2.3.1 Low-frequency limit of the difference signal

Figure 11a shows the vacuum chamber with the beam in the extreme position near point A. Figure 11b is a projection of a cut through A and B.

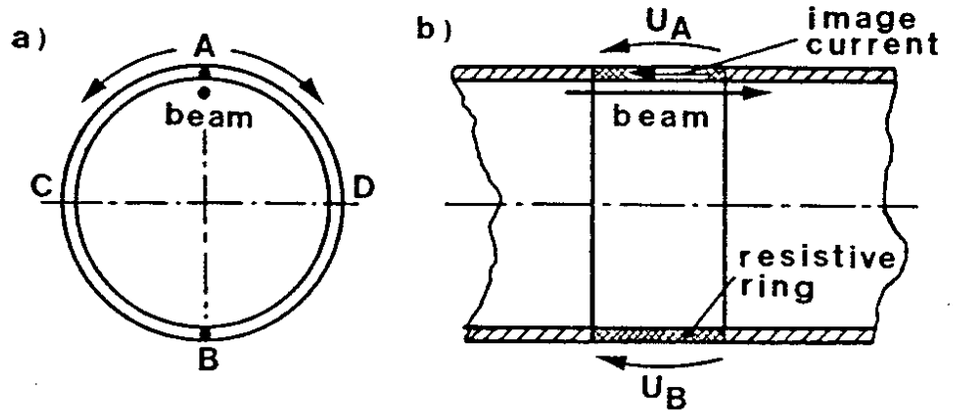

Fig. 11 Vacuum chamber with beam in extreme position

The signal U_A generated in A across the resistive gap is given in Fig. 2 for r = 1. This signal immediately starts to propagate to point B on the two resistive gap lines.

According to the principle that if these signals are sufficiently damped on the lossy line, no signal will appear at point B, then the difference voltage

$$\Delta U = U_A - U_B \tag{25}$$

can be used to determine the beam position. This is only possible for higher frequencies or for short bunches. For a debunched beam (direct current),

$$\Delta U = 0 \ , \tag{26}$$

because a transmission line without longitudinal losses but with transverse insulation losses has no attenuation for a d.c. signal (i.e. $U_A = U_B$).

The lower cut-off frequency is derived in Appendix 3 (Eq. A3.14)

$$\boxed{f_c = \frac{0.111}{L \cdot G \cdot d^2} \ ,} \tag{27}$$

where

L is the line inductance ($\Omega \cdot s/cm$),

G the line conductance ($1/\Omega \cdot cm$),

d the diameter of chamber (cm).

In order to bring the cut-off frequency of the position signal to low values, the line inductance L, the conductance G and diameter d must be large. In other words, the characteristic time constant of the transverse gap line (Eq. A3.15)

$$T_c = L \cdot G \cdot d^2 \cdot \frac{\pi^2}{4} , \qquad (28)$$

which determines the droop of the position signal, must be high.

The conductance G and diameter d can only be increased to certain limits, because the sensitivities of the intensity and position signals will decrease.

The inductance L must be pushed to a maximum.

The condition for obtaining the lower-frequency cut-off of the position signal according to Eq. (27) is that the admittance in parallel with G (external closure) is much smaller than G.

Example: d = 10 (cm), G = 1/30 ($1/\Omega \cdot cm$), L = 3.3 (nH/cm):

$$f_c = \frac{0.111}{3.3 \times 10^{-9}} \frac{30}{100} = 10 \text{ MHz} .$$

2.3.2 Low-frequency limit of the sum signal

This limit would be zero without external closure of the gap.

2.3.3 Upper-frequency limit

Figure 12 shows the resistive ring line of impedance Z with the distributed current sources (arrows)

$$di = q(\ell)\, d\ell . \qquad (29)$$

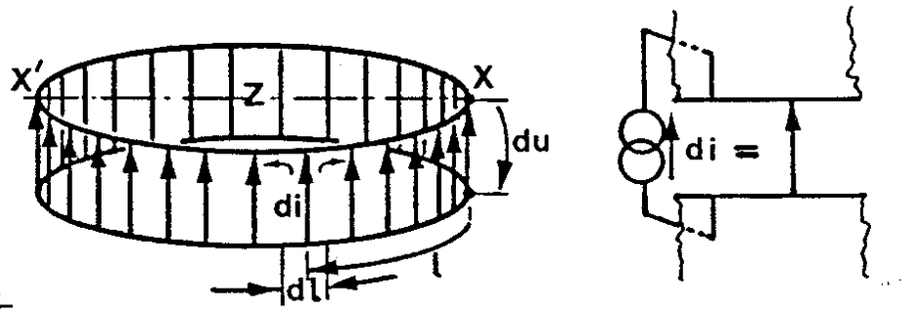

Fig. 12

From each source di alone, there is one wave going to the left and one to the right (each di/2). The voltage generated at the output point x by the source di/2 at a distance ℓ is

$$du = Z\, e^{-\gamma \ell}\, \frac{di}{2} \,. \tag{30}$$

As each current source can contribute not only from distance but also from $\ell + N\lambda$ (λ = circumference, N = 0, 1, 2, ..., ∞), integration to infinity is required. Assuming a symmetric current density distribution $q(\ell)$ with respect to x-x' (beam on the x axis), the left-going and right-going waves give the same contribution, i.e. by superposition

$$\boxed{U = Z \int_0^{\infty} e^{-\gamma \ell}\, q(\ell)\, d\ell \,.} \tag{31}$$

a) *A centred beam* with current I has a constant charge and current distribution versus ℓ ($\varphi = \ell$ for r = 1):

$$q(\ell) = \frac{I}{\lambda} \,, \tag{32}$$

and generates an output voltage [Eq. (31)]

$$U(p) = Z \cdot \frac{I}{\lambda} \cdot \int_0^{\infty} e^{-\gamma \ell}\, d\ell \,; \tag{33}$$

integrated, this gives

$$\boxed{U(p) = Z \cdot \frac{I}{\lambda} \cdot \frac{1}{\gamma} \ .} \qquad (34)$$

Inserting into Eq. (34) the characteristic impedance [9]

$$Z = \sqrt{\frac{(R + pL)}{(G + pC)}} \qquad (35)$$

and the propagation constant γ of Eq. (A3.1), the factor $(R + pL)$ cancels and

$$U(p) = \frac{I(p)}{[(G + pC)\lambda]} = \frac{I(p)}{G\lambda} \cdot \frac{1}{[1 + p(C/G)]} \ . \qquad (36)$$

Equating the real and imaginary part of the denominator leads to the high-frequency limit for a centred beam

$$\boxed{f_{HC} = \frac{\omega_{HC}}{2\pi} = \frac{G}{2\pi C} \ .} \qquad (37)$$

Example: $C = 1$ pF/cm; $G = 1/30\ \Omega \cdot$cm; $\rightarrow f_{HC} = 5.3$ GHz.

A Dirac current input pulse delivers an output signal which decays with $T = C/G = 30$ ps time constant.

b) *An off-centre beam* with the current distribution of Eq. (1) and $r \neq 0$ delivers with Eq. (31) a less simple integral.

But let this problem be considered in another way.

The signals generated by the wall currents travel in both directions around the resistive ring and need a certain propagation time

$$t_p = \frac{d\beta}{d\omega} \ell = \frac{d(\sqrt{\omega GL/2}) \cdot \ell}{d\omega} \qquad (38a)$$

[see Eq. (A3.3b), ℓ = distance between generation and observation] which, differentiated, gives

$$t_p = \frac{1}{2}\sqrt{\frac{GL}{2\omega}}\cdot\ell \quad . \tag{38b}$$

The signal attenuation for a line of length ℓ is [see Eq. (A3.3b)]

$$A = e^{-\alpha\ell} = e^{-(\sqrt{\omega GL/2})\cdot\ell} \quad . \tag{39}$$

From Eq. (39),

$$\ell = -\frac{\ln A}{\sqrt{\omega GL/2}} \tag{40}$$

inserted in Eq. (38b) yields

$$t_p = -\frac{1}{2}\frac{\ln A}{\omega} \quad . \tag{41}$$

The propagation delay which lengthens the output signal (e.g. a Dirac pulse current) depends on the considered frequency and the desired attenuation. It must be shorter than the expected rise-time

$$t_r = \frac{0.35}{f} \quad , \tag{42}$$

i.e.

$$t_p < t_r \quad .$$

Combining Eqs. (41) and (42),

$$-\frac{1}{2}\frac{\ln A}{2\pi f} < \frac{0.35}{f}$$

gives

$$A > e^{-0.35\times 4\pi} = 1.2\% \quad .$$

Only signals from the circumference which contribute with more than 1.2% to the output signal have $t_p < t_r$. Signals contributing with less than 1.2% have $t_p > t_r$.

Example: $f_{max} = 1.5$ GHz, $t_r = 233$ ps, $G = 1/30\ \Omega \cdot cm$, $L = 3.3$ nH/cm.

Let the signal from length ℓ, delayed, contribute 10% to the output signal. Then

$$A = 0.1$$

$$t_p = -\frac{1}{2}\,\frac{\ln 0.1}{2\pi \times 1.5 \times 10^9}$$

$$t_p = 122 \text{ ps}$$

$$t_p < t_r \ .$$

The length which contributes more than 10% from both sides of the output point [Eq. (40)] is

$$\ell = -\frac{\ln A}{\sqrt{\pi f \cdot G \cdot L}} = -\frac{\ln 0.1}{\sqrt{\pi \times 1.5 \times (1/30) \times 3.3}} = 3.2 \text{ cm} \ .$$

From this point of view it seems that there is no upper band limitation: the higher the frequency, the shorter the length and the propagation time. In reality there is the gap capacity C (neglected until now) which limits at

$$f_{max} = \frac{G}{2\pi C} \ , \qquad (43)$$

as for the centred beam [Eq. (37)].

2.4 The frequency-dependent transfer functions of the monitor

The image charge of the beam advances on the chamber wall with the same speed v as the beam (Fig. 13). At the time when the front of the beam reaches the position E, the potential difference between E and F is (for frequencies $f < 0.35 \cdot v/w$):

$$U_{EF} = iR^* \ , \qquad (44)$$

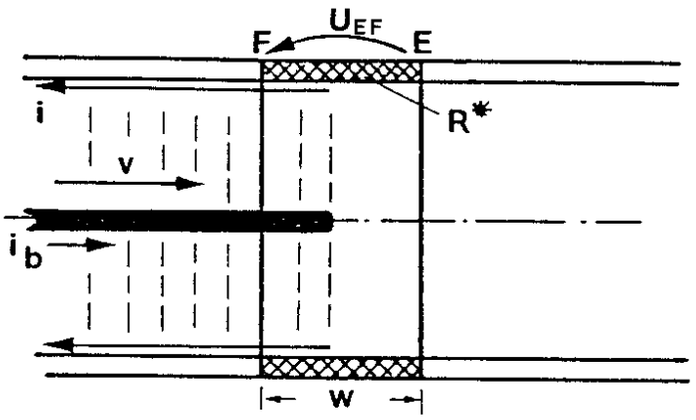

Fig. 13 Beam entering a resistive pick-up

where R^* is complex. The elements which determine R^* are shown in the equivalent circuit (Fig. 14). The ouptput voltage is

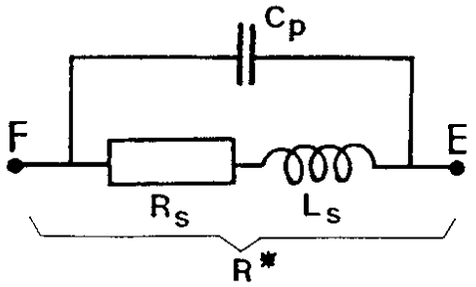

Fig. 14 Equivalent circuit of the resistive pick-up

$$U_{EF} = U(p) = iR_s \frac{1 + pL_s/R_s}{1 + pR_sC_p + p^2L_sC_p}, \qquad (p = j\omega), \qquad (45)$$

or

$$U(p) = iR_s \frac{1 + pTQ^2}{1 + pT + p^2T^2Q^2}, \qquad (46)$$

with

$$Q = \frac{1}{R_s}\sqrt{\frac{L_s}{C_p}}^*, \qquad (47)$$

and

$$T = R_s C_p \ . \tag{48}$$

The transient response in the time domain of a current step input

$$i(p) = \frac{I}{p}$$

is

$$U(t) = IR_s \cdot \mathcal{L}^{-1}\left[\frac{1 + pTQ^2}{p(1 + pT + p^2T^2Q^2)}\right] , \tag{49}$$

where $\mathcal{L}^{-1}$, the inverse Laplace transform, is plotted [11] in Fig. 15 for various quality factors Q and T = 1.

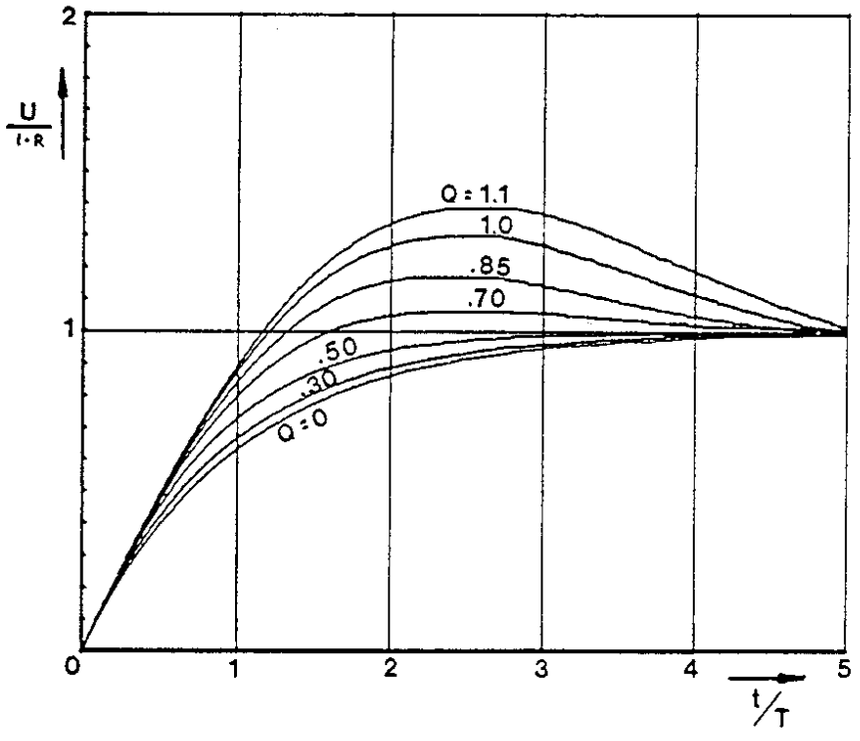

Fig. 15 Signal overshoot versus normalized time for different Q values

The overshoot ratio A/A_- and the relative 90% rise-times τ/τ_0 shown in Fig. 15, are tabulated in Table 1. The aperiodic damping, without overshoot occurs for Q = 0.5. The rise-time is 69% of the uncompensated case. The overshoot of the monitor signal for Q > 0.5 can be used to compensate the capacitance and, partially, the losses of the signal transmission cable.

Table 1

Normalized overshoot and rise-time versus Q values

Q	0	0.3	0.5	0.7	0.85	1	1.1
A/A_{∞}	1	1	1	1.06	1.17	1.30	1.39
τ/τ_0	1.0	0.89	0.69	0.51	0.45	0.43	0.42

The inductance of a homogeneous resistive ring is not high enough (the exterior stored magnetic energy, which determines the inductance, is too small).

Several resistors around the gap increase the inductance, especially when the resistors are long (Fig. 16). Furthermore, the

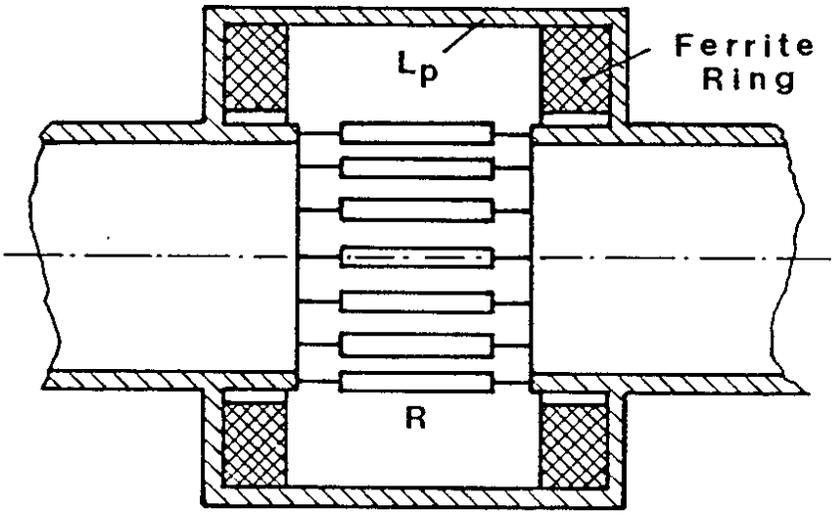

Fig. 16 Cross-section of the monitor with external closure

capacitance of the resistors (and also of the gap) must be small. Several resistors in series decrease the capacitance and increase the inductance as desired.

The low-frequency cut-off of the sum signal depends on the external inductance L_p which is parallel to R_s. The time constant

$$T_1 = \frac{L_p}{R_s}$$

can be increased by ferrite rings (Fig. 16). The total monitor transfer function for the sum signal then becomes

$$F_{1s}(p) = \frac{U}{IR_s} = \frac{pT_1}{1 + pT_1} \frac{1 + pTQ^2}{1 + pT + p^2T^2Q^2} \cdot \qquad (50)$$

The frequency dependence of the transfer function for the difference signal is

$$F_{1d}(p) = K_{1d}(x) \frac{pT_1}{1 + pT_1} \left(1 - \frac{1}{\cosh \sqrt{pT_c}}\right) \frac{1 + pTQ^2}{1 + pT + p^2T^2Q^2} \cdot \qquad (51)$$

The third term of Eq. (51) is derived in Appendix 3 [Eq. (A3.19)]. The second and third terms determine the low-frequency limit, the fourth term the high-frequency cut-off. The constant K_{1d} of the difference signal depends on the beam position x [Eq. (16), $K_{1d} \alpha x$ for small x].

2.5 Signal transmission and optimization

The four signals appearing at the four axis points are connected to wide-band hybrids which deliver the sum and difference signals (Fig. 17). Three filters (Fi) correct these signals before

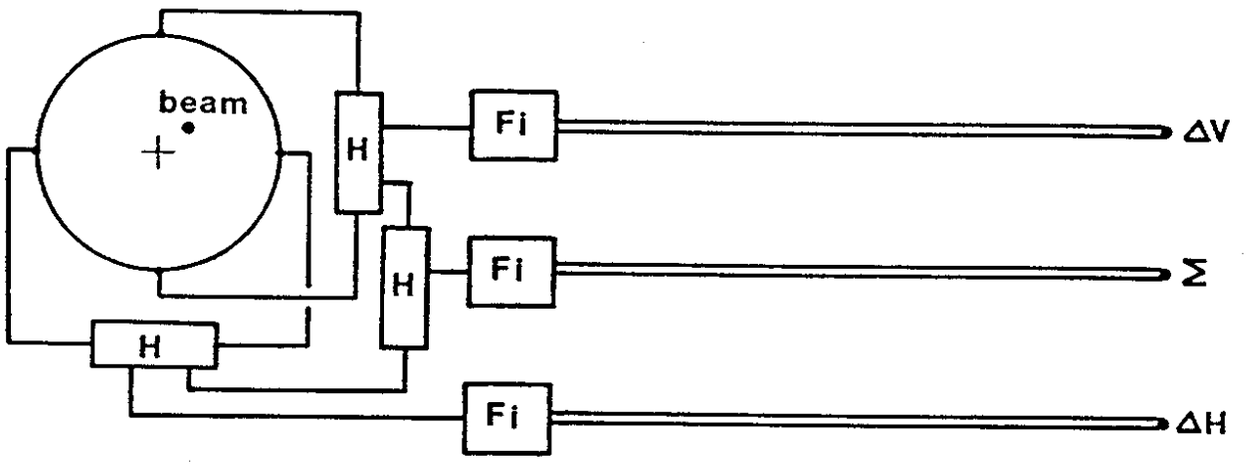

Fig. 17 Schematic diagram of the pick-up and the signal transmission

they are transmitted via high-quality cables to the observation point.

The following block diagram shows the elements with their transfer functions $F_v(p)$, which determine the final signal shape (Fig. 18). The output voltage is

$$U(p) = S(p) \cdot F_1(p) \cdot F_2(p) \cdot F_3(p) \cdot F_4(p) \cdot F_5(p) \ . \tag{52}$$

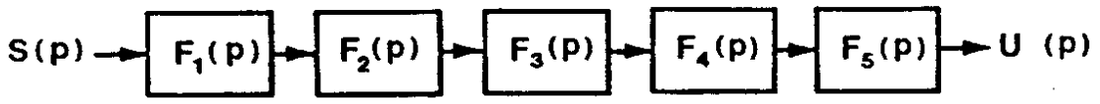

Fig. 18 Block diagram of the signal transmission

In the ideal case, one would expect a theoretical transfer function

$$T(p) = \frac{U(p)}{S(p)} = K \, e^{-p\tau + j\psi} \ , \tag{53}$$

where

τ = total propagation delay (constant),

ψ = phase offset,

K = constant,

$p = j\omega$.

In the case when the amplitude K = const and the group delay is

$$\tau = \frac{d\alpha}{d\omega} = \frac{d(\omega\tau)}{d\omega} = \text{const} \ ,$$

the signal would be transmitted without distortion.

In reality, it is necessary to approach as near as possible

$$F(p) = T(p) = K \, e^{-p\tau + j\psi} \ , \tag{54}$$

where

$$F(p) = F_1(p) \cdot F_2(p) \cdot F_3(p) \cdot F_4(p) \cdot F_5(p) \ . \tag{55}$$

The difference between the vectors F(p) and T(p) is a complex error vector

$$\varepsilon(p) = F(p) - T(p) \ , \tag{56}$$

shown in Fig. 19. At every frequency ω_ν there is an error vector $\varepsilon(j\omega_\nu)$, ($\nu = 1, 2, \ldots, m$).

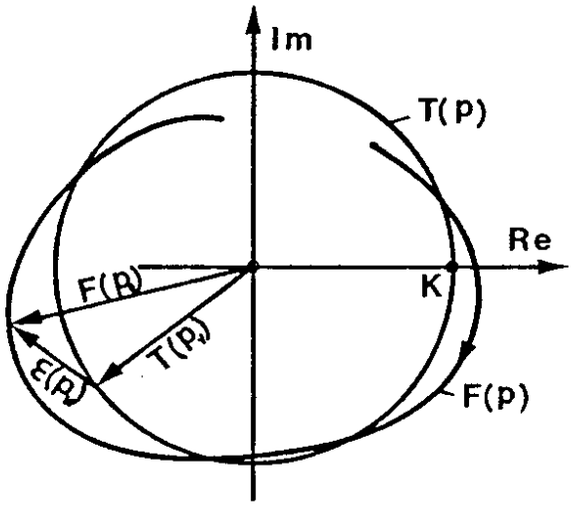

Fig. 19 Signal transfer function in the complex plane

Summing up the squared absolute values of ε for many different frequencies in the desired range gives a total measure for the errors at all interesting frequencies:

$$E = \sum_{\nu=1}^{m} |\varepsilon(j\omega_\nu)|^2 \tag{57}$$

or, with Eq. (56),

$$E = \sum_{\nu=1}^{m} |F(p_\nu) - T(p_\nu)|^2 \ ; \tag{58}$$

E is a real function of all known and unknown variables of $F_\nu(p)$ [see Eq. (55)]. The optimum values of the unknown variables (R_x,

L_x, C_x, T_x, ...) can be found by a computer minimization program (MINUIT) [7] which looks for a minimum of E. The condition is, of course, that all the complex transfer functions $F_v(p)$ are known.

The different transfer functions are discussed in the following, and a summary is shown in Fig. 20.

a) *Monitor*

The monitor transfer functions F_{1s} and F_{1d} were derived in the preceding paragraph [Eqs. (50) and (51)].

b) *Hybrid*

The low- and high-frequency limits of the wide-band hybrids are assumed to be linear first-order expressions:

$$F_2(p) = \frac{pT_2}{(1 + pT_2)} \frac{1}{(1 + pT_3)} ; \qquad (59)$$

T_2: low-frequency cut-off time constant,

T_3: high-frequency cut-off time constant.

Example:

f_2 = 2 MHz,

f_3 = 2 GHz,

$T_2 = 1/2\pi f_2$ = 79.6 ns,

$T_3 = 1/2\pi f_3$ = 79.6 ps.

c) *Filter*

The filter transfer function $F_3(p)$ is determined in Appendix 4 [Eq. (A4.8)]. The variables are C_1, C_2, R_1, and R_2.

d) *Cable*

The transfer function of a transmission line, which has only conductor losses (skin effect), can be described by [12]

$$F_4(p) = \frac{U_2}{U_1} = e^{-(1+j)\alpha\ell} = e^{-\sqrt{pT_0}} , \qquad (60)$$

with

$$T_0 = \frac{(\alpha\ell)^2}{\pi f} \qquad (61)$$

= rise-time 0-48%;

$\alpha\ell$ = attenuation exponent of line with length ℓ (in neper = 1 Np = 8.686 dB);

f = frequency at the attenuation $\alpha\ell$.

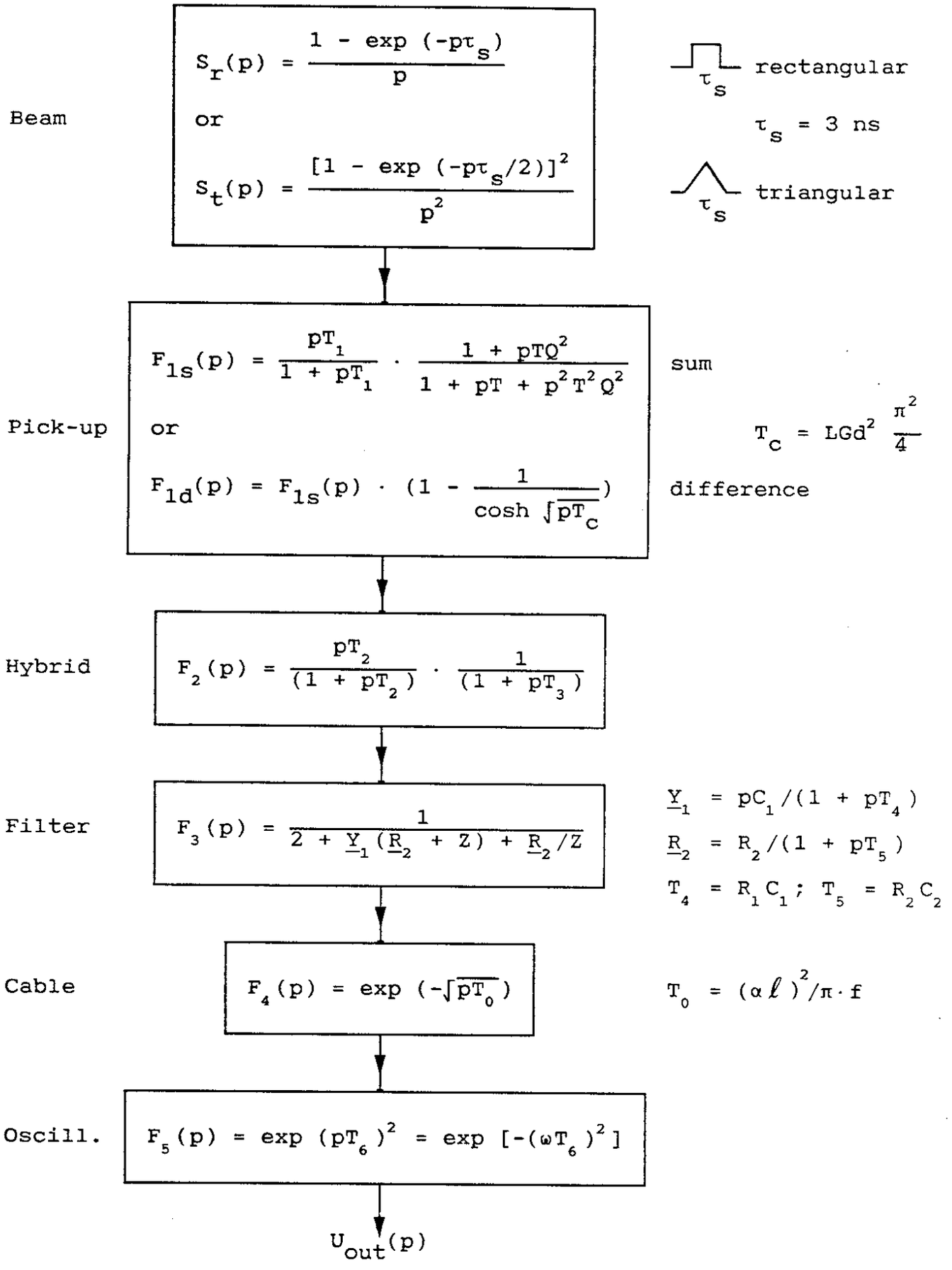

Fig. 20 Flow chart of signal transmission with transfer functions

Example: ℓ = 100 m, 4 dB/100 m attenuation at 1 GHz, $\alpha\ell$ = 4/8.686 = 0.4606 Np, $T_0 = (0.4606)^2/(\pi \times 1 \times 10^9) = 67.5$ ps.

e) *Oscilloscope*

It is assumed that the oscilloscope has a Gaussian attenuation

$$F_5(p) = e^{(pT_6)^2} = e^{-(\omega T_6)^2} \quad . \tag{62}$$

Example: attenuation of 3 dB at 1 GHz:

$$T_6 = \frac{\sqrt{-\ln (1/\sqrt{2})}}{2\pi f} = 93.7 \text{ ps} \quad .$$

The product of the complex transfer functions*) [Eq. (55)] is computed in a FORTRAN subroutine FCN (Appendix 5A) with eight unknown variables,

X(1) = K amplitude of theoretical function [Eq. (53)],
X(2) = τ propagation delay [Eq. (53)],
X(3) = Q pick-up factor [Eq. (47)],
X(4) = R_1 resistance
X(5) = R_2 resistance
X(6) = C_1 capacitance
X(7) = C_2 capacitance
} of filter [Appendix 4, Fig. A4.1, Eq. (A4.8)]
X(8) = ψ initial phase offset [Eq. (53)],

for 30 frequencies (10 per decade) between 2 MHz and 2 GHz in constant logarithmic steps:

$$AUG = \sqrt[30]{\frac{f_{max}}{f_{min}}} \tag{63}$$

or

$$AUG = 1.25892541 \quad .$$

The absolute values of the difference vectors [Eq. (58)] had to be normalized with K^2 [X(1)**2] as the difference vectors are proportional to K^2 (to avoid K = 0 solution).

---

*) Except the oscilloscope transfer function.

The sum E of the 30 squared and normalized absolute values of the difference vectors is fed to MINUIT [7] version MINTLD (double precision) and minimized by varying all eight unknown variables $X_1, \ldots, X_8$.

The starting values, initial step sizes, and lower and upper limits of the eight variables are listed below the FORTRAN program (Appendix 5A).

The output of this program is given in Appendix 5B. After 192 calls it finds a minimum for FCN. The values of the parameters are circled. The value of K = 0.35 corresponds to about 3 dB attenuation (0.35/0.5 = 0.7 ≙ -3 dB).

For higher attenuations, i.e. smaller K values, there exist deeper minima, but the output signals become smaller.

A good compromise is investigated in Appendix 6 with the LAPLACE program [12]. (R_1, R_2, C_1, and C_2 are underlined.)

The spectrum of a rectangular input pulse of length τ_s,

$$S_r(p) = \frac{1 - e^{-p\tau_s}}{p}, \qquad (p = j\omega), \tag{64}$$

is transformed by each transfer function F_v (v = 1 to 5) (see Fig. 20) and the inverse Laplace transform is performed. The output of a 3 ns input pulse is shown below the FORTRAN subroutine in Appendix 6 (Fig. A6.1).

The output of a 3 ns triangular input pulse with spectrum

$$S_t(p) = \frac{\left[1 - e^{-p(\tau_s/2)}\right]^2}{p^2} \tag{65}$$

is shown in Appendix 6 (Fig. A6.2) for the same transfer function parameters.

Appendices 7 and 8 give the FORTRAN INPUTS and OUTPUTS for the *difference signal* as do Appendices 5 and 6 for the *sum signal*.

3. MECHANICAL DESIGN

Figure 21 shows the monitor with three 180° hybrids (ANZAC H9, 2 MHz-2 GHz) which produce the sum and difference signals. The hybrids are connected to the resistor ring via four coaxial cables

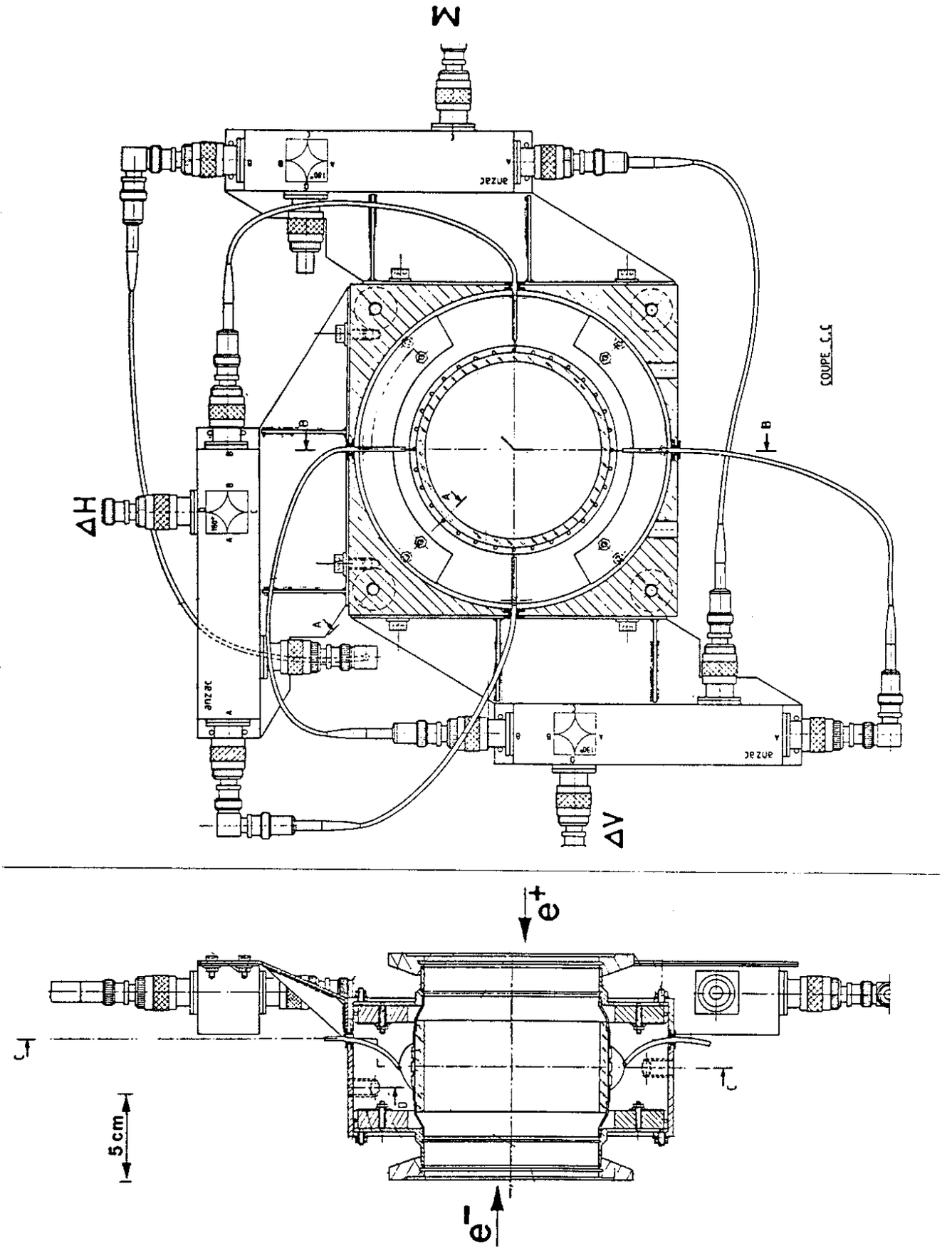

Fig. 21 Mechanical layout of the monitor

(RG58) of equal length. The ring is composed of 96 resistors, 32 parallel groups of 3 in series on the periphery. The three series resistors (3 x 10 Ω metal film) bridge the 4 cm gap between two tubes of 100 mm diameter. A ceramic tube of 5 mm thickness makes the gap vacuum-tight. To avoid charging effects, the inner surface of the tube is metallized with antimony (300 Ω over gap).

The outer cavity contains two ferrite (2E8) rings. The inductance of these rings in parallel with the total gap resistance determines the lower cut-off frequency of the intensity signal.

Further remarks:

- There are three resistors in series to decrease the parasitic capacitance and increase the inductance.
- The inductance L of the transverse gap-line increases with the gap width. In order to obtain a low cut-off frequency, the gap width was pushed to the maximum.
- The hybrids are placed as near as possible to the resistor ring to reduce the cable lengths to the minimum.

A length difference of 0.3 mm limits the beam position resolution for 1 GHz at 0.5 mm.

Figure 22 shows the assembled monitor.

4. TEST BENCH

4.1 Mechanical test device

Figure 23 shows the monitor in the measurement device, which is a 3 m long brass tube of 100 mm inner diameter. The rectangular flanges on both ends allow linear transverse displacements of an inner wire (1 mm) or tube (ϕ = 20 mm). A fast pulse or step-pulse generator (reflectometer) feeds the inner conductor through one flange.

Unavoidable reflection at the perpendicular end flanges was eliminated by time-filtering or windowing. This means that the reflected signals are well separated in time from the direct signals owing to the relatively long travelling time in the tube.

The filters for cable loss compensation are located directly at the hybrid outputs.

A cable of 100 m length is required for the transmission of the signals between the monitor and the observation room.

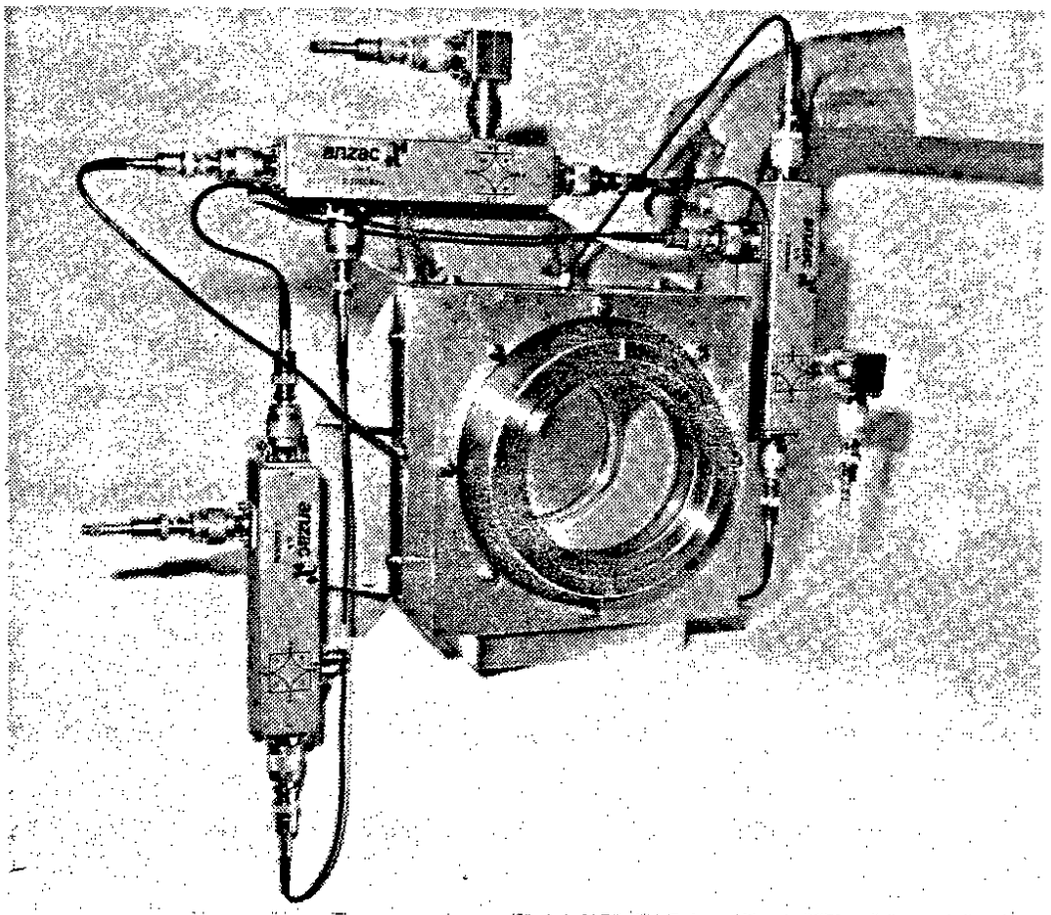

Fig. 22 Photo of monitor with hybrids

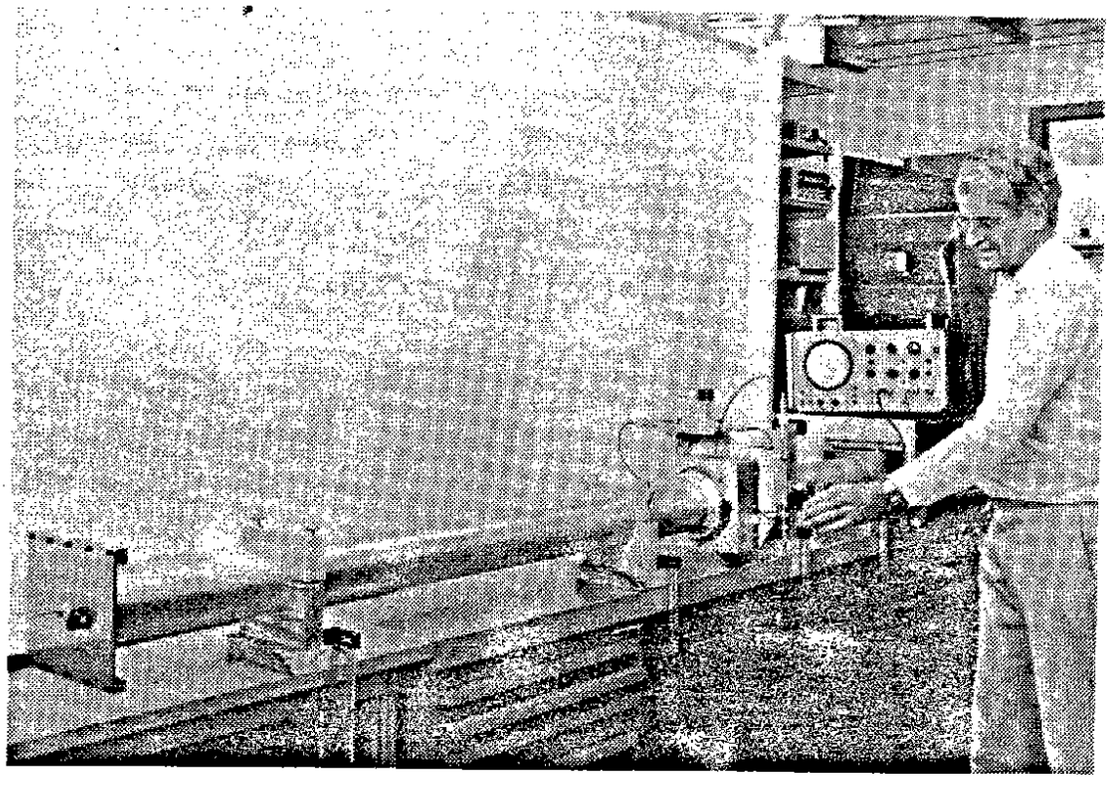

Fig. 23 Laboratory test bench

The coaxial cable chosen, with enough waveguide mode margin for f_{max} = 1.5 GHz, is a 7/8-inch Flexwell cable [4 dB/100 m attenuation at 1 GHz]. As this cable is unwieldy, a thinner and shorter cable with the same total attenuation was used in the laboratory for the filter optimization.

Rotation of the monitor with respect to the displacement plane allows to simulate the beam in any point of the cross-section.

4.2 Laboratory results

The monitor was tested with short pulses and with step pulses.

a) The pulse generator signal is shown in Fig. 24 (upper trace, 47 dB attenuated). The modulated pulse has about 3 ns length.

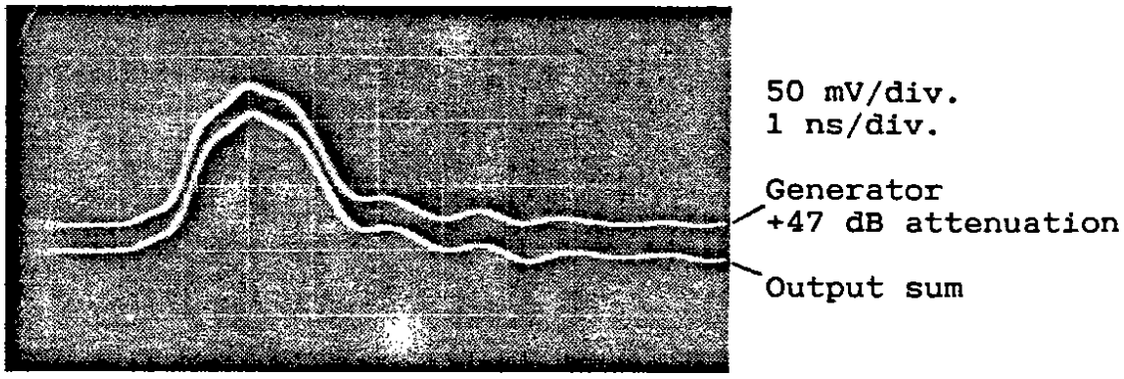

Fig. 24 Input and sum output of the transmission system

The sum output [via monitor, hybrids, filter, cable, and sampling scope (TEK. 1S1)] is shown in the lower trace. The pulse shape of the generator is well reproduced. The difference signals for three simulated beam positions (+15, 0, -15 mm) are given in Fig. 25. The zero position resolution is about 0.3 mm.

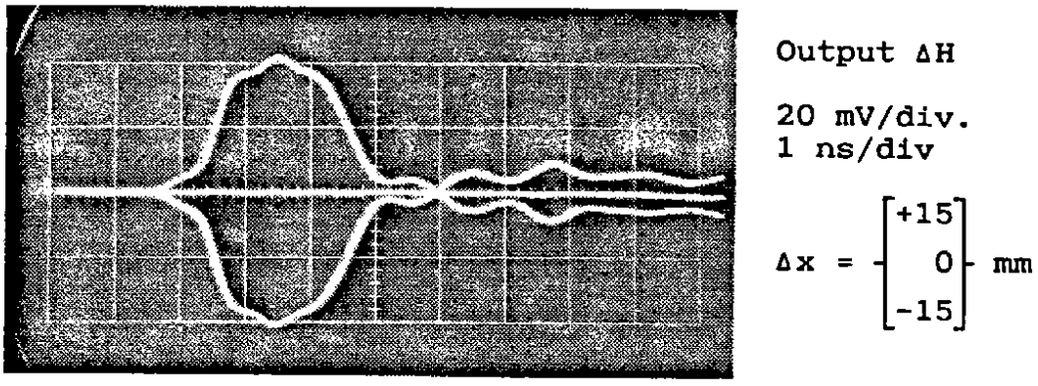

Fig. 25 Difference output signals for three beam positions

b) The step-pulse generator (S52), belonging to the TDR sampler (TEK. 7S12), with the sampling head (S6), has a rise-time of about 35 ps.

The overall difference and sum signals are shown in Fig. 26.

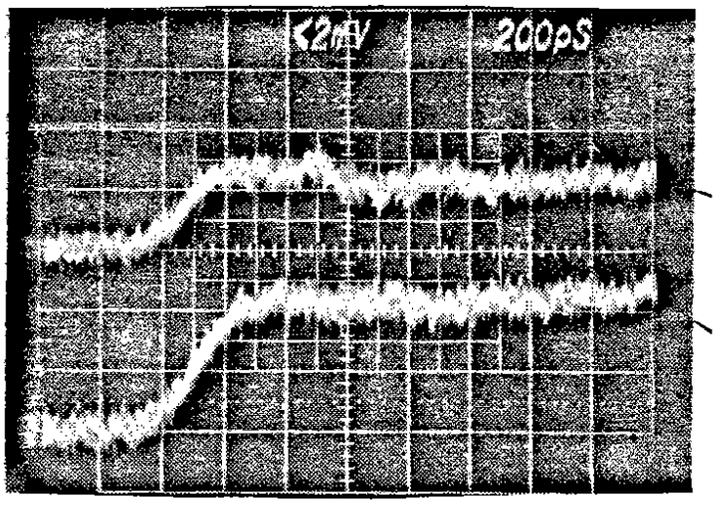

Fig. 26 Difference and sum output signals for a step input of 35 ps rise-time

Owing to the small generator step-height (200 mV) and the small total gap resistance (0.94 Ω), the output signals are also small and are noisy.

The droop of the signals can be seen in Fig. 27.

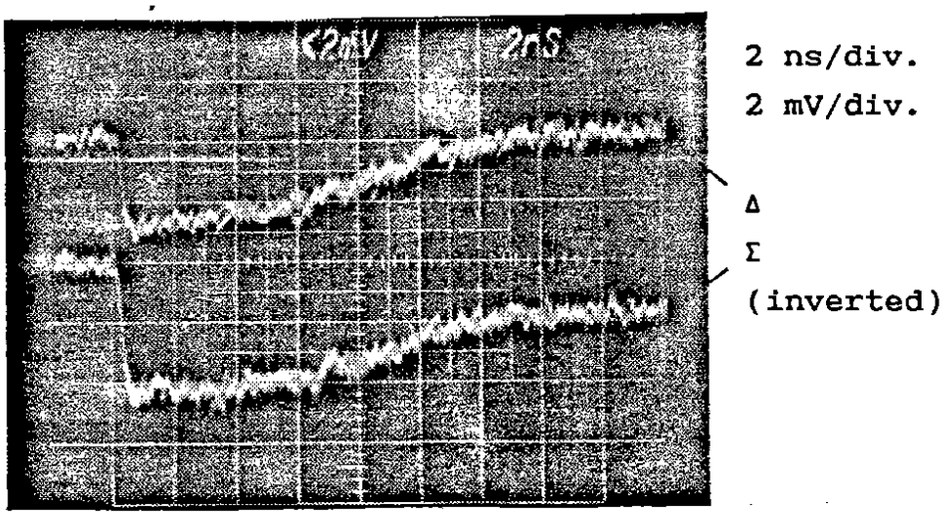

Fig. 27 Droop of difference and sum output signals

The measured rise-times (τ_r), fall-time constants (T_f), and cut-off frequencies are given in Table 2.

Table 2

Rise- and fall-times and frequency limits for the sum and difference signal

	τ_r (ps)	T_f (ns)	$f_H = 0.35/\tau_r$ (GHz)	$f_L = 1/2\pi T_f$ (MHz)
Σ	230	17	1.52	2.65
Δ	210	60	1.66	9.36

5. RESULTS WITH BEAM

Typical signals of the wide-band monitor installed in the EPA are shown in Figs. 28 to 30. The signals are observed with a 1 GHz

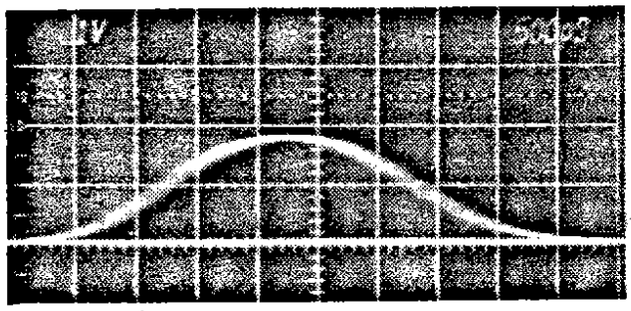

Σ(3×10^{10} p/p)

1 V/div.
500 ps/div.

Fig. 28 Sum signal of stacked e^- beam

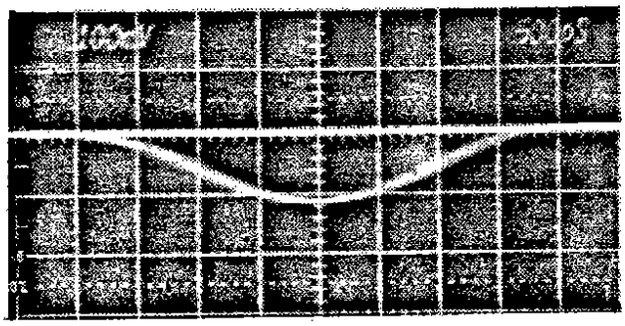

ΔH
Δx = -2.4 mm

100 mV/div.
500 ps/div.

Fig. 29 Horizontal difference signal

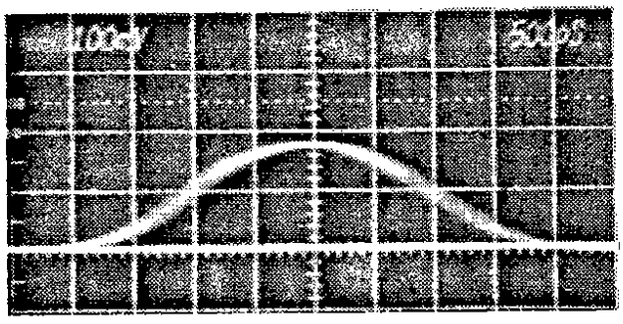

ΔV
Δy = 4 mm

100 mV/div.
500 ps/div.

Fig. 30 Vertical difference signal

oscilloscope (TEK. 7A29/7104) at the end of a 100 m long, 7/8-inch Flexwell cable. The low frequencies are cut at 68 kHz by a series miniature condenser (47 nF) at the input of the oscilloscope (reflection < 2%).

Figure 31 shows the superimposed horizontal position signals for eight beam positions obtained by varying a dipole current.

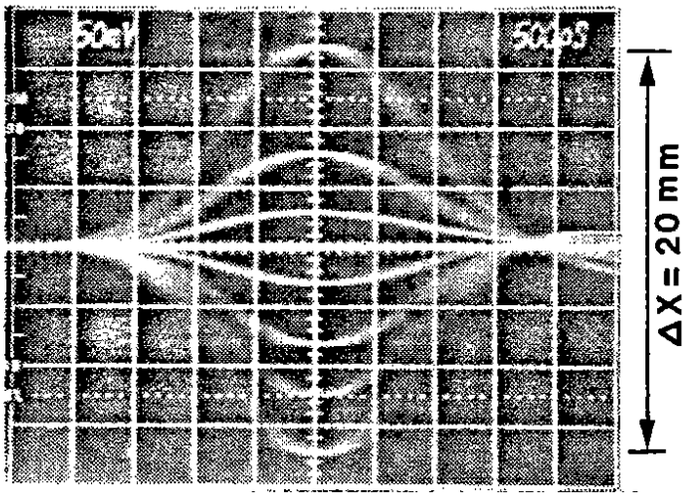

ΔH
(eight beam positions by modulated bump)

50 mV/div.
500 ps/div.

Fig. 31 Eight superimposed horizontal beam-position signals

Figure 32 shows a 'mountain-range' display of a coupled-bunch instability (caused by the coupling impedances) which starts, for

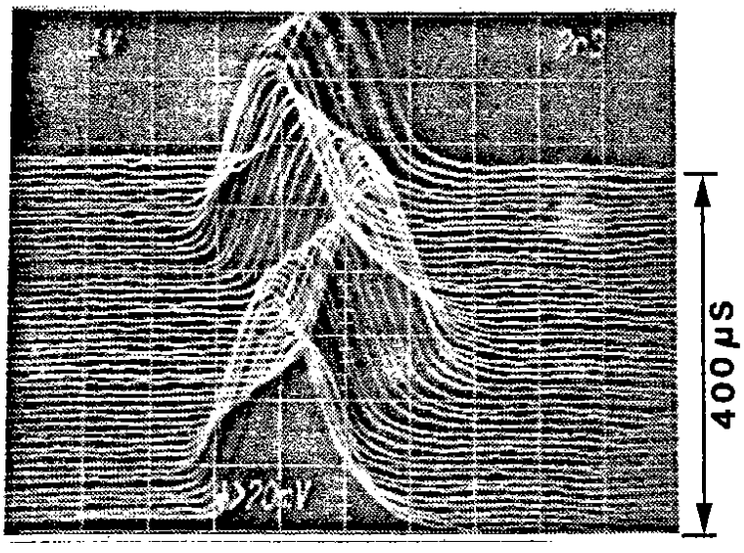

Σ

1 V/div.
2 ns/div.

Fig. 32 Sum signal during instability
(coupled bunch instability)

eight circulating bunches, at about 2 x 10^{11} (total) particles, and produces, at 4 x 10^{11} particles, coherent phase oscillations during 400 μs, as displayed. (The noise on the base lines comes from the mountain-range trigger unit.)

6. CLOSING REMARKS

The study and realization of this monitor has shown that it is possible to measure with this type of apparatus not only the longitudinal structure but also the transverse beam position in a wide frequency range. The lower-frequency limit f_L of the position signal, which in the case under consideration is 9.4 MHz, could be further decreased by increasing the chamber diameter, the inductance and/or the conductance of the transverse gap line. Doubling the diameter would give $f_L' = f_L/4 = 2.35$ MHz.

Trials to increase the inductance L of the gap line by ferrite loading of the gap were less effective.

The high-frequency limits are given essentially by the hybrids and the transmission cables and by the cable connections to the gap.

7. CHARACTERISTICS

The characteristics of the total system, i.e. monitor, hybrids, filters, and 100 m cables, are as follows:

Signal bandwidth of	
intensity	2.7 MHz - 1.5 GHz
position	9.4 MHz - 1.6 GHz
Sensitivity on	
beam current	1.26 mV/mA
intensity (4σ = 2.8 ns)	1.1 V/10^{10} particles per bunch
position	$40 \cdot \Delta U/\Sigma U$ mm
Resolution on	
intensity	< 5 x 10^6 particles per bunch
position	0.5 mm
Error (for r < 20 mm)	
on beam linearity	< 5%
on beam intensity	< 5%
(see also §2.)	
Coupling impedance $\lvert Z/n \rvert$	< 0.2 Ω
Rise-time of	
intensity signal	230 ps
difference signal	210 ps
Characteristic cable impedance	50 Ω
Reflections (1 MHz - 1.5 GHz)	< 3%
Hybrids H9 ANZAC	2 MHz - 2 GHz
Total gap resistance	0.94 Ω

Acknowledgements

It is a pleasure to thank A. Krusche and H. Kugler for stimulating discussions, D. Fiander for his support, M. Corcelle for the mechanical design, and P. Pelletier for the assembly of the monitors.

Appendix 1

DERIVATION OF SUM OF Q VERSUS BEAM POSITIONS r and χ

From Eqs. (5) to (8), i.e.

$$q_1 = \frac{1 - r^2}{1 + r^2 - 2r \cos \chi} \tag{A1.1}$$

$$q_3 = \frac{1 - r^2}{1 + r^2 + 2r \cos \chi} \tag{A1.2}$$

$$q_2 = \frac{1 - r^2}{1 + r^2 - 2r \sin \chi} \tag{A1.3}$$

$$q_4 = \frac{1 - r^2}{1 + r^2 + 2r \sin \chi} \tag{A1.4}$$

$$\Sigma q = q_1 + q_3 + q_2 + q_4$$

$$= (1 - r^2) \left[\frac{2(1 + r^2)}{(1 + r^2)^2 - (2r \cos \chi)^2} + \frac{2(1 + r^2)}{(1 + r^2)^2 - (2r \sin \chi)^2} \right] \tag{A1.5}$$

$$\Sigma q = (1-r^2)2(1+r^2)\ x$$

$$\left[\frac{(1+r^2)^2 - 4r^2 \sin^2 \chi + (1+r^2)^2 - 4r^2 \cos^2 \chi}{(1+r^2)^4 - (1+r^2)^2 4r^2 \sin^2 \chi - (1+r^2)^2 4r^2 \cos^2 \chi + 16r^4 \cos^2 \chi \sin^2 \chi} \right] \tag{A1.6}$$

$$\boxed{\Sigma q = \frac{4(1 - r^8)}{(1 - r^4)^2 + 16\, r^4 \cos^2 \chi \sin^2 \chi}\ ,} \tag{A1.7}$$

or in rectangular coordinates with Eq. (3),

$$\Sigma q(x,y) = \frac{4[1 - (x^2 + y^2)^4]}{[1 - (x^2 + y^2)^2]^2 + 16x^2y^2} . \qquad (A1.8)$$

Appendix 2

INTEGRATION OF THE CHARGE-DISTRIBUTION INTEGRAL

From Eq. (20)

$$Q_v = \int_{\varphi_1}^{\varphi_2} \frac{(1 - r^2)\, d\varphi}{1 + r^2 - 2r \cos(\varphi - \chi)} . \tag{A2.1}$$

Using the addition theorem for the cosine term, we get

$$Q_v = (1 - r^2) \int_{\varphi_1}^{\varphi_2} \frac{d\varphi}{1 + r^2 - 2r \cos\chi \cos\varphi - 2r \sin\chi \sin\varphi} . \tag{A2.2}$$

Putting

$$\begin{aligned} a &= 1 + r^2 , \\ b &= -2r \cos\chi , \\ c &= -2r \sin\chi , \end{aligned} \tag{A2.3}$$

$$Q_v = (1 - r^2) \int_{\varphi_1}^{\varphi_2} \frac{d\varphi}{a + b \cos\varphi + c \sin\varphi} . \tag{A2.4}$$

This equation transformed with Ref. [8a] gives

$$Q_v = (1 - r^2) \int_{\Phi_1}^{\Phi_2} \frac{d\Phi}{a + p \cos\Phi} , \tag{A2.5}$$

with

$$p = \frac{b}{\cos\chi} = -2r \tag{A2.6}$$

and

$$\Phi = \varphi - \chi \ . \tag{A2.7}$$

Equation (A2.5) integrated with Ref. [8b] and using Eq. (A2.7) yields

$$Q_v = 2 \operatorname{arctg} \left[\frac{1 + r}{1 - r} \operatorname{tg} \left\{ \frac{\varphi - \chi}{2} \right\} \right] \Bigg|_{\varphi_1}^{\varphi_2} , \tag{A2.8}$$

or

$$\boxed{Q_v = 2 \cdot \left\{ \operatorname{arctg} \left[\frac{1 + r}{1 - r} \operatorname{tg} \left\{ \frac{\varphi_2 - \chi}{2} \right\} \right] - \operatorname{arctg} \left[\frac{1 + r}{1 - r} \operatorname{tg} \left\{ \frac{\varphi_1 - \chi}{2} \right\} \right] \right\} ,} \tag{A2.9}$$

where the limits φ_1 and φ_2 depend on Q_1 to Q_4 as given in Eq. (21).

Appendix 3

LOWER CUT-OFF FREQUENCY OF THE BEAM-POSITION SIGNAL

The general propagation constant of a transmission line is [9]

$$\gamma = \sqrt{(R + pL)(G + pC)} \; ; \qquad \text{(A3.1)}$$

R: resistance
L: inductance
G: conductance
C: capacitance
} per unit length of line

$p = j\omega$.

Assuming that for the gap line we have small copper losses

$$R << |pL|$$

and high insulation losses

$$G >> |pC| \; ,$$

then

$$\gamma = \sqrt{pLG} = \sqrt{j\omega LG} \; . \qquad \text{(A3.2)}$$

with

$$\sqrt{j} = e^{j(\pi/4)} = \frac{1}{\sqrt{2}} (1 + j) \; ,$$

$$\gamma = \alpha + j\beta = \sqrt{\frac{\omega LG}{2}} (1 + j) \; , \qquad \text{(A3.3a)}$$

where

$$\alpha = \sqrt{\frac{\omega LG}{2}} \; ; \quad \beta = \sqrt{\frac{\omega LG}{2}} \; . \qquad \text{(A3.3b)}$$

An input signal U_A is attenuated through a lossy open-ended transmission line of length ℓ, and becomes [9]

$$U_B = \frac{U_A}{\cosh (\alpha + j\beta)\ell} \; . \qquad \text{(A3.4)}$$

Or with Eq. (A3.3a),

$$\frac{U_B}{U_A} = \frac{1}{\cosh\,[(1 + j)\alpha\ell]} \cdot \tag{A3.5}$$

At the lower-frequency limit, the difference voltage

$$\Delta U = U_A - U_B \tag{A3.6}$$

is attenuated by 3 dB with respect to U_A:

$$|\Delta U| = |U_A - U_B| = \frac{|U_A|}{\sqrt{2}} \cdot \tag{A3.7}$$

Dividing Eq. (A3.7) by U_A and combining with Eq. (A3.5) gives

$$\left|1 - \frac{1}{\cosh\,[(1 + j)\alpha\ell]}\right| = \frac{1}{\sqrt{2}} \cdot \tag{A3.8}$$

The complex function between the absolute signs is plotted via a computer program [10] for $\alpha\ell$ as the variable (see Fig. A3.1). At the crossing point with the circle

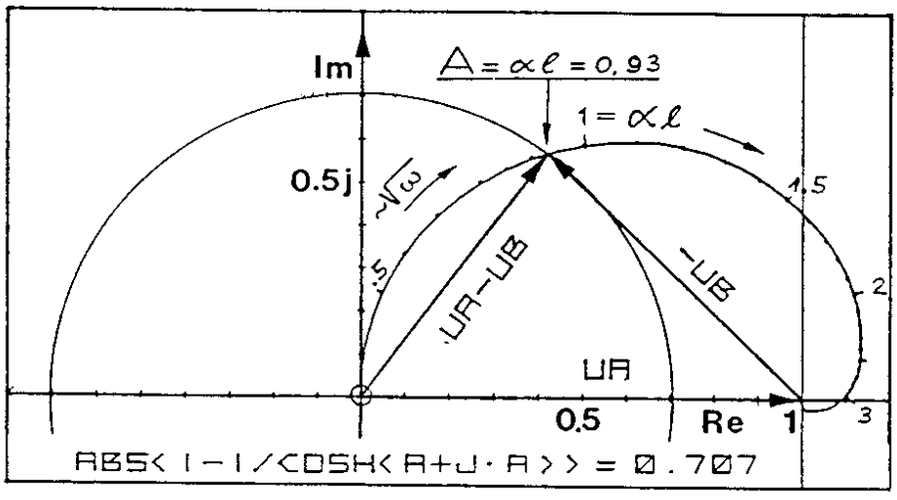

Fig. A3.1 Graphical solution of Eq. (A3.8)

$$\underline{r} = \frac{1}{\sqrt{2}} e^{j\varrho} \quad , \tag{A3.9}$$

the solution can be read:

$$\boxed{\alpha\ell = 0.93 \ .} \tag{A3.10}$$

From Eq. (A3.3b)

$$\alpha\ell = \sqrt{\frac{1}{2} \omega_c LG \cdot \ell} \quad , \tag{A3.11}$$

and the cut-off frequency is

$$f_c = \frac{\omega_c}{2\pi} = \frac{(0.93)^2}{LG\ell^2\pi} \quad , \tag{A3.12}$$

or with

$$\ell = \frac{d\pi}{2} \tag{A3.13}$$

(d is the diameter of the vacuum chamber),

$$\boxed{f_c = \frac{(0.93)^2 \ x \ 4}{\pi^3 LGd^2} = \frac{0.111}{LGd^2} \quad ,} \tag{A3.14}$$

and with

$$T_c = LG\ell^2 = LG \frac{d^2\pi^2}{4} \quad , \tag{A3.15}$$

$$f_c = \frac{(0.93)^2}{\pi T_c} = \frac{0.275}{T_c} \ . \tag{A3.16}$$

Example: d = 10 cm, G = 1/15 Ω·cm, L = 1.75 nH/cm

$$T_c = 1.75 \times \frac{1}{15} \times 100 \times \frac{\pi^2}{4} = 28.78 \text{ ns} ,$$

$$f_c = \frac{0.275}{28.78 \times 10^{-9}} = 9.55 \text{ MHz} .$$

A chamber diameter of d = 20 cm would lead to a lower cut-off frequency, $f_c' = f_c/4 = 2.39$ MHz.

Remark

Two parallel lines have the same product

$$L_p G_p = L_s G_s = LG \qquad \text{(A3.17)}$$

as a single line because the conductance doubles and the inductance is halved (coupling neglected).

From Eqs. (A3.5) and (A3.6)

$$\frac{\Delta U}{U_A} = 1 - \frac{1}{\cosh\,[(1 + j)\alpha\ell]} , \qquad \text{(A3.18)}$$

which can be simplified with Eqs. (A3.3a) and (A3.15), and with

$$\omega = -jp ,$$

$$1 + j = \sqrt{2}\, e^{j(\pi/4)} ,$$

and

$$\sqrt{-j} = e^{-j(\pi/4)} ,$$

to read

$$\boxed{\frac{\Delta U}{U_A} = 1 - \frac{1}{\cosh \sqrt{pT_c}} .} \qquad \text{(A3.19)}$$

Appendix 4

FILTER TRANSFER FUNCTION

For the compensation of the HF cable losses and the LF monitor losses the circuit of Fig. A4.1 is assumed.

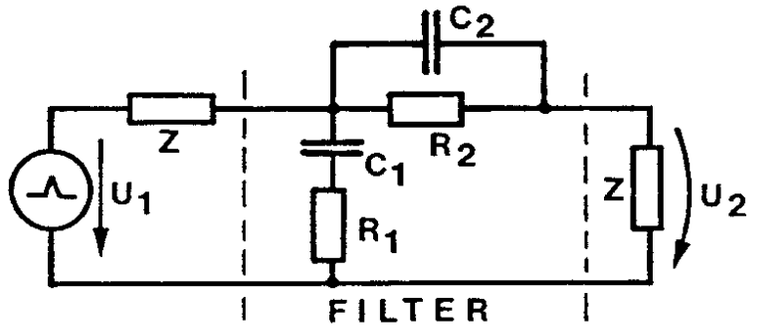

Fig. A4.1 Cable loss correction filter.

The input and output signals are linked by the following matrix product:

$$\begin{bmatrix} U_1 \\ I_1 \end{bmatrix} = \begin{bmatrix} 1 & Z \\ 0 & 1 \end{bmatrix} \begin{bmatrix} a_{11} & a_{12} \\ a_{21} & a_{22} \end{bmatrix} \begin{bmatrix} U_2 \\ I_2 \end{bmatrix} \qquad (A4.1)$$

corresponding to the source and filter matrices. The matrix elements of the filter (see two-port theory) are:

$$a_{11} = 1 + \frac{\underline{R}_2}{Z} \qquad (A4.2)$$

$$a_{21} = \frac{1}{\underline{R}_1} + \frac{1}{Z} + \frac{1}{Z}\frac{\underline{R}_2}{\underline{R}_1} , \qquad (A4.3)$$

with

$$\underline{R}_1 = R_1 + \frac{1}{pC_1} , \qquad (A4.4)$$

$$\underline{R}_2 = \frac{R_2}{1 + pC_2R_2} . \qquad (A4.5)$$

The voltage ratio U_1/U_2 is obtained by the first element of the resulting product matrix (as $I_2 = 0$):

$$\frac{U_1}{U_2} = a_{11} + Za_{21} \quad . \tag{A4.6}$$

Inserting Eq. (A4.2) and (A4.3) into Eq. (A4.6), we have

$$\frac{U_1}{U_2} = 1 + \frac{\underline{R}_2}{Z} + \frac{Z}{\underline{R}_1} + 1 + \frac{\underline{R}_2}{\underline{R}_1} \quad . \tag{A4.7}$$

The inverse transfer function is

$$\boxed{\frac{U_2}{U_1} = \frac{1}{2 + \underline{Y}_1(\underline{R}_2 + Z) + (\underline{R}_2/Z)} = F_3(p)} \tag{A4.8}$$

where

$$\underline{Y}_1 = \frac{1}{\underline{R}_1} = \frac{pC_1}{1 + pT_4} \quad , \tag{A4.9}$$

$$\underline{R}_2 = \frac{R_2}{1 + pT_5} \quad , \tag{A4.10}$$

$$T_4 = R_1 C_1 \quad , \tag{A4.11}$$

and

$$T_5 = R_2 C_2 \quad . \tag{A4.12}$$

Appendix 5

A) FORTRAN SUBROUTINE OF 'MINUIT' PROGRAM FOR PICK-UP SUM SIGNAL OPTIMIZATION

```
      CALL MINTLD
      STOP
      END

      SUBROUTINE FCN(NPAR,G,F,X,IFLAG)
      IMPLICIT DOUBLE PRECISION (A-H, O-Z)
      DIMENSION X(8)
      COMPLEX G,TH,P,V,Y

      DATA T/.03/,T0/.0675/,T1/100./,T2/79.6/,T3/.0796/,T6/.0937/
      DATA Z/50./,FMIN/.002/,AUG/1.25892541/

      FR=FMIN/AUG
      F=0

      DO 10 I=1,30
      FR=FR*AUG
      OM=FR*6.283185308
      P=(0.,1.)*OM
      G=(P*T1)*(1.+P*T*X(3)**2)/((1.+P*T1)*(1.+P*T+P*P*T*T*X(3)**2))
      G=G*P*T2/((1.+P*T2)*(1.+P*T3))
      V=X(5)/(1.+P*X(5)*X(7))
      Y=P*X(6)/(1.+P*X(4)*X(6))
      G=G/(2.+Y*(V+Z)+V/Z)
      G=G*CDEXP(-CDSQRT(P*T0))

      TH=X(1)*CDEXP((0.,-1.)*OM*X(2))*CDEXP((0.,1.)*X(8))
   10 F=F+(CABS(G-TH))**2/(X(1)**2)

      RETURN
      END
PICK UP OPTIMIZATION
           1     K          0.35        .05        0.3          1.
           2     TAU        0.1         .001       0.         100.
           3     Q          1.6         .1         0.           1.6
           4     R1         200.        20.      100.        9000.
           5     R2          16.         1.        1.          50.
           6     C1        0.200      0.47E-2      0.          1.
           7     C2        0.47E-1    0.10E-2      0.          1.
           8     PHI       0.3        0.0785

ERROR DEF   0.1
SEEK
MINIMIZE
PRINTOUT   1.

EXIT
```

B) OUTPUT OF 'MINUIT' OPTIMIZATION PROGRAM (SUM SIGNAL)

FCN VALUE	CALLS	TIME	EDM
0.3262861E+01	192	0.00	0.67E+00

INT.	EXT.	PARAMETER	VALUE
1	1	K	0.35069E+00
2	2	TAU	0.12024E+00
3	3	Q	0.15993E+01
4	4	R1	0.17890E+03
5	5	R2	0.17146E+02
6	6	C1	0.20518E+00
7	7	C2	0.47336E-01
8	8	PHI	0.18616E+00

MIGRAD MINIMIZATION HAS CONVERGED

Appendix 6

A) COMPLEX TRANSFER FUNCTION OF 'LAPLACE' PROGRAM FOR SUM SIGNAL TRANSMISSION WITH OPTIMUM FILTER PARAMETERS (3 ns RECTANGULAR INPUT)

```
C
      COMPLEX FUNCTION SPECTR(S)
      COMPLEX S,G,V,Y
      DATA T/.03/,T0/.0675/,T1/100./,T2/79.6/,T3/.0796/,T6/.0937/
      DATA Z/50./,Q/1.6/,R1/200.0/R2/16.0/,C1/.200/,C2/.047/
      DATA TS/3./

C-----TRIANGULAR INPUT PULSE
C     SPECTR=((1.-CEXP(-S*TS/2))**2)/(S*S)
C-----RECTANGULAR INPUT PULSE
      SPECTR=(1.-CEXP(-S*TS))/S
      SPECTR=SPECTR*(S*T1)*(1+S*T*Q*Q)
      SPECTR=SPECTR/((1.+S*T1)*(1.+S*T+S*S*T*T*Q*Q))
      SPECTR=SPECTR*S*T2/((1.+S*T2)*(1.+S*T3))
      V=R2/(1.+S*R2*C2)
      Y=S*C1/(1.+S*R1*C1)
      SPECTR=SPECTR/(2.+Y*(V+Z)+V/Z)
      SPECTR=SPECTR*CEXP(-CSQRT(S*T0))
      SPECTR=SPECTR*CEXP(S*S*T6*T6)
      SPECTR=SPECTR*CEXP(1.5*S)

      RETURN
      END

10.       1   RECTANGULAR INPUT PULSE     (OPT. 3)
```

Fig. A6.1 Time response output for a 3 ns input pulse.

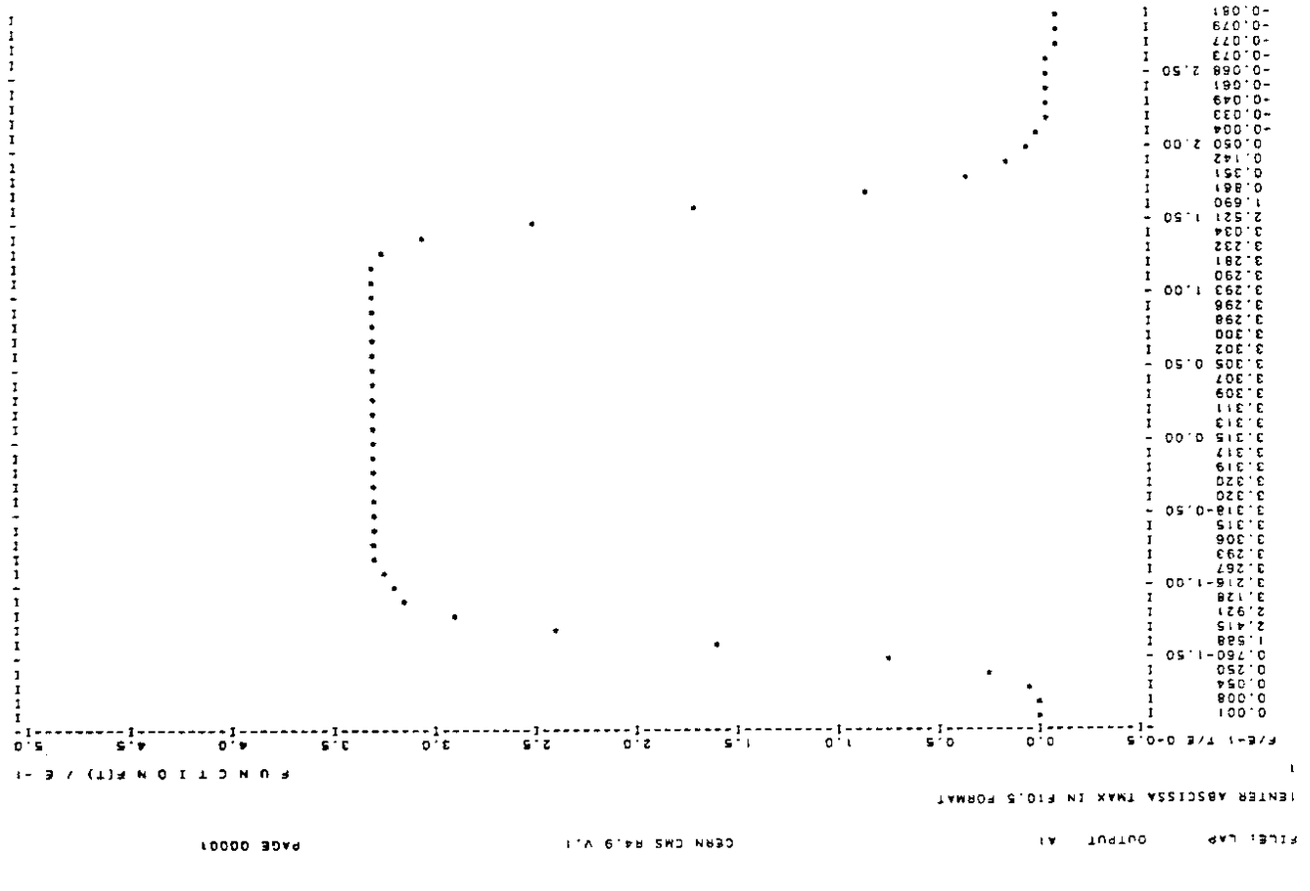

B) COMPLEX TRANSFER FUNCTION FOR OPTIMUM FILTER PARAMETERS (3 ns TRIANGULAR INPUT)

```
C
      COMPLEX FUNCTION SPECTR(S)
      COMPLEX S,G,V,Y
      DATA T/.03/,T0/.0675/,T1/100./,T2/79.6/,T3/.0796/,T6/.0937/
      DATA Z/50./,Q/1.6/,R1/200.0/R2/16.0/,C1/.200/,C2/.047/
      DATA TS/3./

C-----TRIANGULAR INPUT PULSE
      SPECTR=((1.-CEXP(-S*TS/2))**2)/(S*S)
C-----RECTANGULAR INPUT PULSE
C     SPECTR=(1.-CEXP(-S*TS))/S
      SPECTR=SPECTR*(S*T1)*(1+S*T*Q*Q)
      SPECTR=SPECTR/((1.+S*T1)*(1.+S*T+S*S*T*T*Q*Q))
      SPECTR=SPECTR*S*T2/((1.+S*T2)*(1.+S*T3))
      V=R2/(1.+S*R2*C2)
      Y=S*C1/(1.+S*R1*C1)
      SPECTR=SPECTR/(2.+Y*(V+Z)+V/Z)
      SPECTR=SPECTR*CEXP(-CSQRT(S*T0))
      SPECTR=SPECTR*CEXP(S*S*T6*T6)
      SPECTR=SPECTR*CEXP(1.5*S)

      RETURN
      END

10.         1    TRIANGULAR INPUT PULSE     (OPT. 3)
```

Fig. A6.2 Time response output for a 3 ns triangular input pulse.

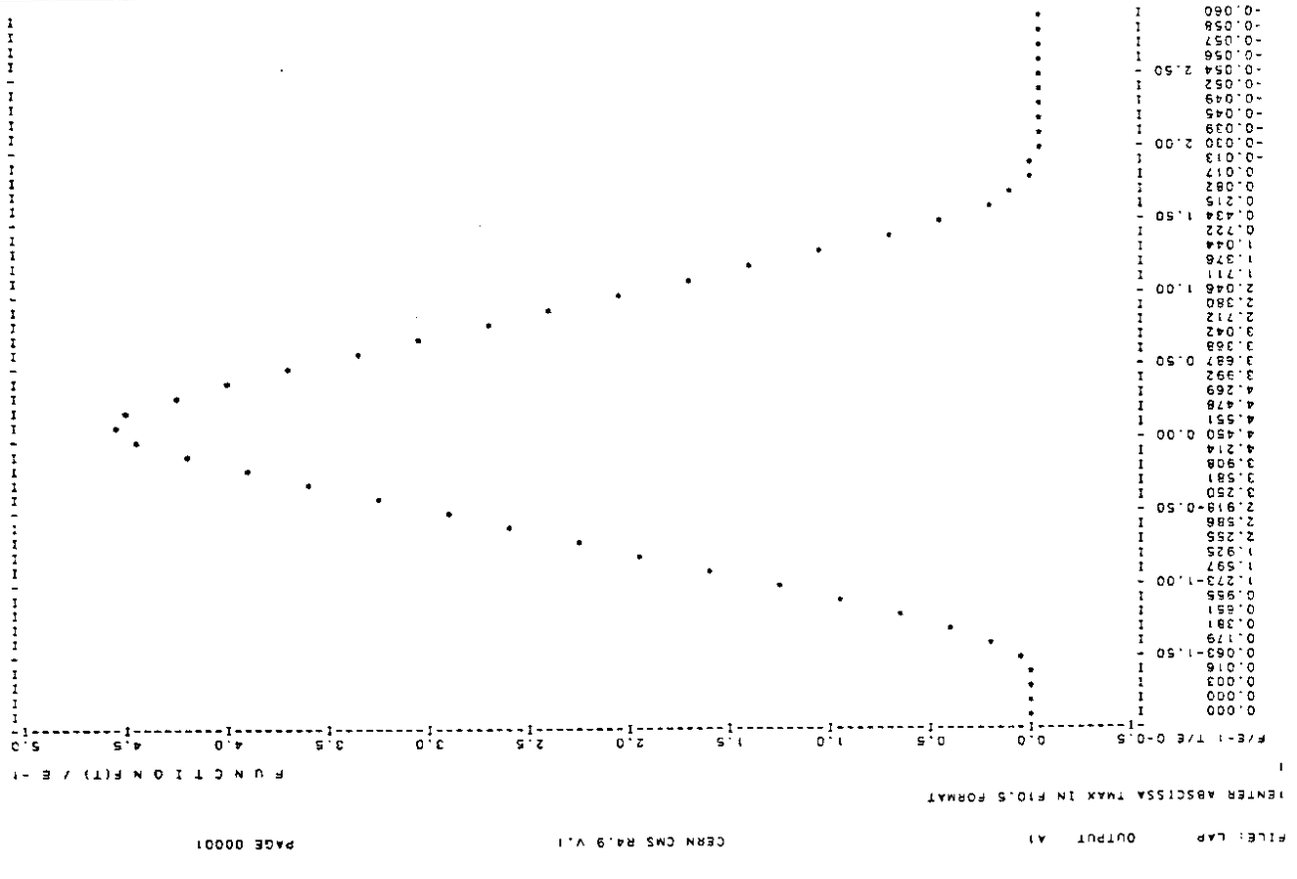

Appendix 7

A) FORTRAN SUBROUTINE OF 'MINUIT' FOR DIFFERENCE SIGNAL OPTIMIZATION

```
      CALL MINTLD
      STOP
      END

      SUBROUTINE FCN(NPAR,G,F,X,IFLAG)
      IMPLICIT DOUBLE PRECISION (A-H, O-Z)
      DIMENSION X(8)
      COMPLEX G,TH,P,V,Y

      DATA T/.03/,T0/.0675/,T1/100./,T2/79.6/,T3/.0796/,T6/.0937/
      DATA Z/50./,FMIN/.010/,AUG/1.25892541/,TC/28.78/

      FR=FMIN/AUG
      F=0

      DO 10 I=1,20
      FR=FR*AUG
      OM=FR*6.283185308
      P=(0.,1.)*OM
      G=(P*T1)*(1.+P*T*X(3)**2)/((1.+P*T1)*(1.+P*T+P*P*T*T*X(3)**2))
      G=G*(1.-2./(CDEXP(CDSQRT(P*TC))+CDEXP(-CDSQRT(P*TC))))
      G=G*P*T2/((1.+P*T2)*(1.+P*T3))
      V=X(5)/(1.+P*X(5)*X(7))
      Y=P*X(6)/(1.+P*X(4)*X(6))
      G=G/(2.+Y*(V+Z)+V/Z)
      G=G*CDEXP(-CDSQRT(P*T0))

      TH=X(1)*CDEXP((0.,-1.)*OM*X(2))*CDEXP((0.,1.)*X(8))
   10 F=F+(CABS(G-TH))**2/(X(1)**3)

      RETURN
      END
PICK UP OPTIMIZATION
          1     K          0.35        .05        0.3         1.
          2     TAU        0.1         .001       0.        100.
          3     Q          1.6         .1         0.          1.6
          4     R1         200.        20.      100.       9000.
          5     R2          16.         1.        1.         50.
          6     C1        0.200     0.47E-2      0.          1.
          7     C2       0.47E-1    0.10E-2      0.          1.
          8     PHI        0.3       0.0785

ERROR DEF   0.1
SEEK
MINIMIZE
PRINTOUT   1.

EXIT
```

B) 'MINUIT' OUTPUT, DIFFERENCE SIGNAL OPTIMIZATION

FCN VALUE	CALLS	TIME	EDM
0.5968709E+01	214	0.00	0.15E+02

INT.	EXT.	PARAMETER	VALUE
1	1	K	0.41116E+00
2	2	TAU	0.14055E+00
3	3	Q	0.15961E+01
4	4	R1	0.21003E+03
5	5	R2	0.18741E+02
6	6	C1	0.10208E+00
7	7	C2	0.66641E-01
8	8	PHI	0.23173E+00

Appendix 8

A) COMPLEX TRANSFER FUNCTION 'LAPLACE' FOR DIFFERENCE SIGNAL TRANSMISSION WITH OPTIMUM FILTER PARAMETERS (3 ns RECTANGULAR INPUT)

```
C
      COMPLEX FUNCTION SPECTR(S)
      COMPLEX S,G,V,Y
      DATA T/.03/,T0/.0675/,T1/100./,T2/79.6/,T3/.0796/,T6/.0937/
      DATA Z/50./,Q/1.6/,R1/210.0/R2/18.7/,C1/.102/,C2/.066/,TC/28.78/
      DATA TS/3./

C-----TRIANGULAR INPUT PULSE
C     SPECTR=((1.-CEXP(-S*TS/2))**2)/(S*S)
C-----RECTANGULAR INPUT PULSE
      SPECTR=(1.-CEXP(-S*TS))/S
      SPECTR=SPECTR*(S*T1)*(1+S*T*Q*Q)
      SPECTR=SPECTR/((1.+S*T1)*(1.+S*T+S*S*T*T*Q*Q))
      SPECTR=SPECTR*(1.-2./(CEXP(CSQRT(S*TC))+CEXP(-CSQRT(S*TC))))
      SPECTR=SPECTR*S*T2/((1.+S*T2)*(1.+S*T3))
      V=R2/(1.+S*R2*C2)
      Y=S*C1/(1.+S*R1*C1)
      SPECTR=SPECTR/(2.+Y*(V+Z)+V/Z)
      SPECTR=SPECTR*CEXP(-CSQRT(S*T0))
      SPECTR=SPECTR*CEXP(S*S*T6*T6)
      SPECTR=SPECTR*CEXP(1.5*S)

      RETURN
      END

10.         1    RECTANGULAR INPUT PULSE     (OPT. 4)
```

Fig. A8.1 Time response output for a 3 ns input pulse.

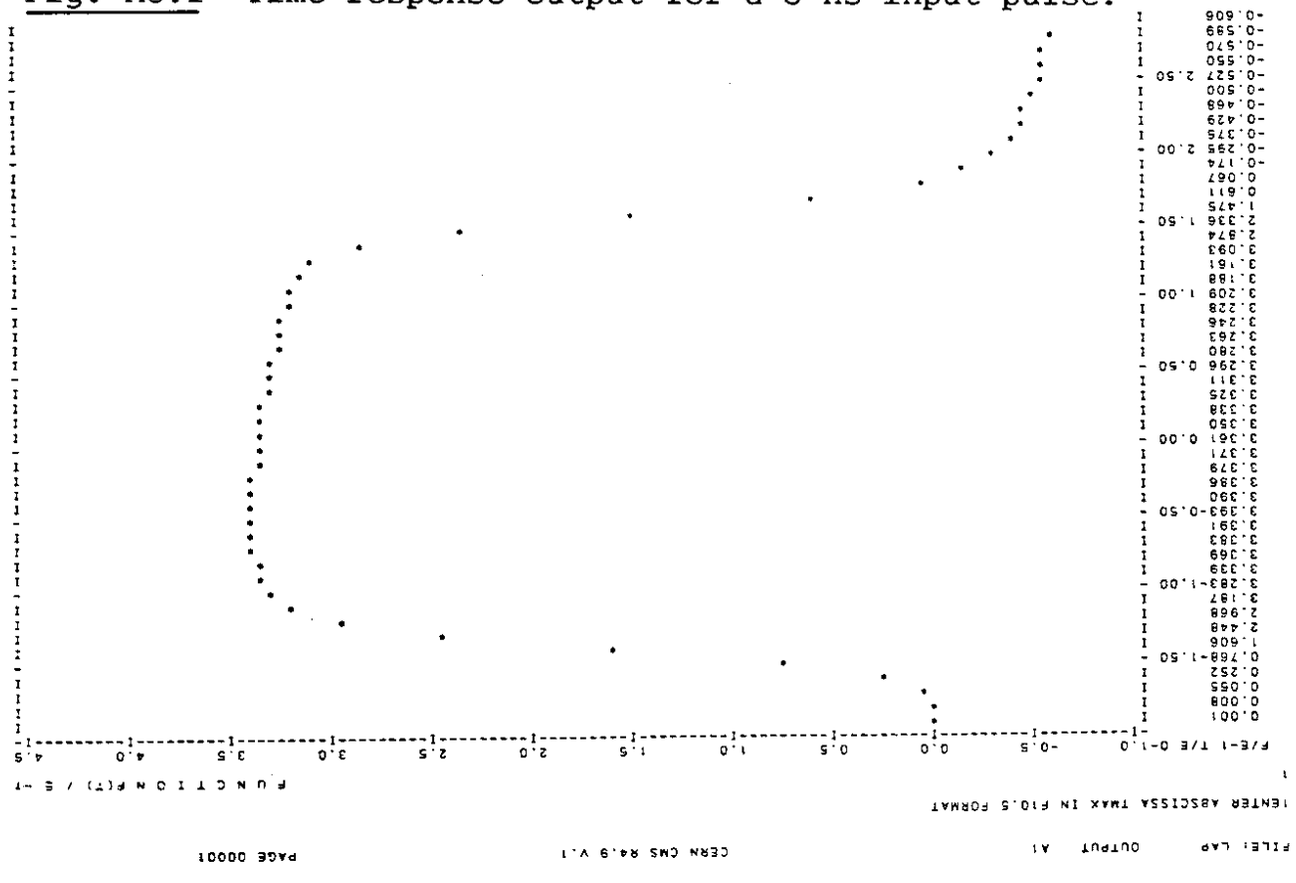

B) COMPLEX TRANSFER FUNCTION FOR OPTIMUM FILTER PARAMETERS (3 ns TRIANGULAR INPUT)

```
C
      COMPLEX FUNCTION SPECTR(S)
      COMPLEX S,G,V,Y
      DATA T/.03/,T0/.0675/,T1/100./,T2/79.6/,T3/.0796/,T6/.0937/
      DATA Z/50./,Q/1.6/,R1/210.0/R2/18.7/,C1/.102/,C2/.066/,TC/28.78/
      DATA TS/3./

C-----TRIANGULAR INPUT PULSE
      SPECTR=((1.-CEXP(-S*TS/2))**2)/(S*S)
C-----RECTANGULAR INPUT PULSE
C     SPECTR=(1.-CEXP(-S*TS))/S
      SPECTR=SPECTR*(S*T1)*(1+S*T*Q*Q)
      SPECTR=SPECTR/((1.+S*T1)*(1.+S*T+S*S*T*T*Q*Q))
      SPECTR=SPECTR*(1.-2./(CEXP(CSQRT(S*TC))+CEXP(-CSQRT(S*TC))))
      SPECTR=SPECTR*S*T2/((1.+S*T2)*(1.+S*T3))
      V=R2/(1.+S*R2*C2)
      Y=S*C1/(1.+S*R1*C1)
      SPECTR=SPECTR/(2.+Y*(V+Z)+V/Z)
      SPECTR=SPECTR*CEXP(-CSQRT(S*T0))
      SPECTR=SPECTR*CEXP(S*S*T6*T6)
      SPECTR=SPECTR*CEXP(1.5*S)

      RETURN
      END

10.       1   TRIANGULAR INPUT PULSE     (OPT. 4)
```

Fig. A8.2 Time response output for a 3 ns triangular input pulse.

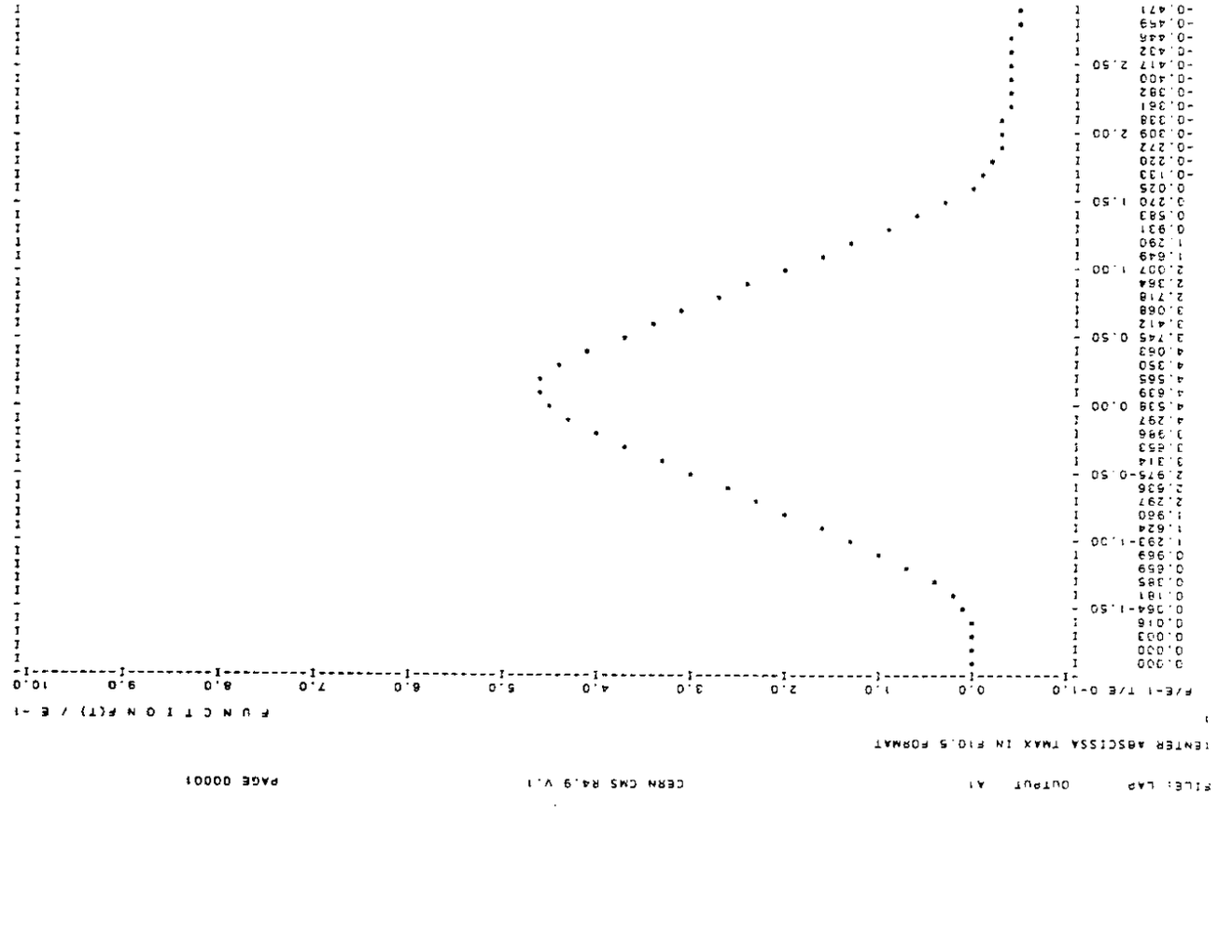

REFERENCES

[1] D. Blechschmidt, J.P. Delahaye and D.J. Warner, LEP pre-injector parameter list, CERN PS/LPI/Note 83-28 (1983).

[2] G. Schneider, The new pick-up electrodes for the CPS, CERN MPS/Int. RF 65-9 (1965), p. 32 [Eq. (15)].

[3] R.T. Avery, A. Faltens and E.C. Hartwig, Non-intercepting monitor of beam current and position, UCRL-20166 (1971).

[4] G.C. Schneider, Messwerterfassung und Ubertragung zur Strahllagebestimmung beim 28 GeV Protonen-Synchrotron von CERN, Dissertation, Technische Universität Hannover (1971), p. 12.

[5] R. Bossart, Analysis and performance of the wall-current monitor for the SPS, CERN Lab II-CO/Int./BM 75-2 (1975).

[6] G.C. Schneider, Proposal for a resistive non-destructive UHF wide-band pick-up station with beam position measurement, CERN MPS/SR/Note 73-32 (1973).

[7] F. James and M. Roos, Function minimization program 'MINUIT', D506, CERN Program Library (1967).

[8] Hütte I, Theoretische Grundlagen (Verlag v. Wilhelm Ernst & Sohn, Berlin, 1955), a) p. 96, formula (33); b) p. 95, formula (30).

[9] Reference data for radio engineers, 5th edition (Howard W. Sams & Co. Inc., Indianapolis/Kansas City/New York, 1972), pp. 22-2 and 22-3.

[10] H.H. Umstätter, Conformal mapping program, CUC No. 638 (HP 9820A) (1976).

[11] T. Miski, Transient response programme, CUC No. 403 (HP 9820A) (1975).

[12] H.H. Umstätter, LAPLACE program, unpublished.